3-14-2019

Wettability of fully hydroxylated and alkylated (001) α-quartz surface in carbon dioxide atmosphere

Aleksandr Abramov
Edith Cowan University, a.abramov@ecu.edu.au

Alireza Keshavarz
Edith Cowan University, a.keshavarz@ecu.edu.au

Stefan Iglauer
Edith Cowan University, s.iglauer@ecu.edu.au

10.1021/acs.jpcc.9b00263
This document is the Accepted Manuscript version of a Published Work that appeared in final form in *The Journal of Physical Chemistry C*, as:

Abramov, A., Keshavarz, A., & Iglauer, S. (2019). Wettability of fully hydroxylated and alkylated (001) alpha-quartz surface in carbon dioxide atmosphere. *The Journal of Physical Chemistry C, 123*(14), 9027–9040.

Wettability of Fully Hydroxylated and Alkylated (001) alpha-Quartz Surface in Carbon Dioxide Atmosphere

Aleksandr Abramov*, Stefan Iglauer, Alireza Keshavarz, School of Engineering, Edith Cowan University, 270 Joondalup Drive, Joondalup, WA 6027, Western Australia, Australia

*aabramov@our.ecu.edu.au

Abstract

Wettability of alkylated quartz surface is of primary importance in several technological applications including the development of oil and gas reservoirs and carbon geo-sequestration. It is intuitively understood and experimentally confirmed that hydroxylated quartz surface is hydrophilic. By gradually saturating hydroxylated (001) alpha-quartz surface with pentyl groups we show using molecular dynamics simulations that the surface can also exhibit extreme hydrophobicity. Within a range of surface pentyl group density from 0.29 to 3.18 per nanometre squared the contact angle of a water droplet under 10 MPa pressure of carbon dioxide at 300 K changes from 10-20 to 180 degrees. This study has shown that a complete description of wettability of alkylated quartz surface requires three contact angles, one at the tip level of pentyl groups, and two at the level of quartz surface. The latter two are the contact angle of the spherical droplet and the hidden contact angle of a water "skirt" formed between the tip level of pentyl groups and the quartz surface. Analysis of the hidden contact angle unveils a binary wettability, where the surface relatively abruptly transforms from hydrophilic (the contact angle is less than 90 degrees) to hydrophobic (the contact angle is 180 degrees) with an increase in surface pentyl group concentration.

Introduction

In oil and gas reservoirs and in saline aquifers mineral surfaces are exposed to water and hydrocarbons over geological time scales [1-2]. Hydroxylation and chemisorption of hydrocarbons with following change in wettability is thus expected and was demonstrated experimentally [3]. Because of natural abundance of quartz its wettability is of primary importance for carbon geo-sequestration and recovery of hydrocarbons.

Properties of quartz crystal and its surfaces are of key importance in many areas, including the construction industry, piezoelectric devices [4], biotoxicity [5], astrochemistry [6] and the geology of the solid earth [7]. Depending on conditions of pressure and temperature, crystalline silica (SiO_2) can form different polymorphs, some of them are α- and β-quartz, α- and β-cristobalite and coesite [8]; structures and properties of these polymorphs are known and understood. Low temperature polymorphs, such as α-quartz, exist at ambient conditions. Above approximately 3 GPa and 1200°C α-quartz becomes unstable and with increase in pressure transforms to coesite, and with increase in temperature transforms to β-quartz [9].

The (001) surface of α-quartz is regarded as the most stable surface of pristine [10] and hydroxylated α-quartz [11-12]. Thus, numerous research studies have been dedicated to understanding the properties of these quartz surfaces using computational chemistry and materials science methods [10-17].

Contemporary (001) α-quartz surface models consider two extremes in terms of the degree of surface hydroxylation, namely (i) the pristine (no hydroxyl groups, stable Si-O-Si bridges) and (ii) the hydroxylated model. The ideal fully hydroxylated theoretical silica surface is covered with geminal silanol groups, which results in OH group (or single silanol group) concentration of 9.4 per nm^2 [18] (slightly depends on calculated/measured lattice constants). However, any real hydroxylated silica

surface (excluding possible contaminations and defects) is a combination of isolated silanols, vicinal silanols, geminal silanols and Si-O-Si bridges [19]. Average OH group (or single silanol group) concentration on real hydroxylated surfaces under ambient conditions amounts to 4.5-6.2 per nm^2 [20]. This silanol density aligns with data reported in a comprehensive review paper, where the average concentration of OH groups is said to be a physicochemical constant of 4.6 or 4.9 groups per nm^2, depending on the averaging technique, the least square or the arithmetical mean, respectively [19].

In recent years one specific factor - the wettability of quartz surfaces, has been intensively studied because of its implications in carbon capture and storage technology where it determines reliability, security and capacity of the structural and the residual trapping mechanisms [1, 21]. Quartz abundance in the Earth's continental crust (the second most abundant mineral after feldspars with weight concentration of 12% [22-23]) and in cap rocks (more than 50% by weight [1]) makes it crucial for characterisation of the overall wettability of real multi-mineral cap rocks. In addition, sandstone reservoirs, mainly made up of quartz, are prime targets for CO2 storage [24].

Experimental wettability studies of quartz surfaces have explored different gaseous atmospheres including air [25-27], hydrogen sulphide and carbon dioxide e.g. [28-29]. Various water solutions have been tested ranging from distilled water [30] to brines of different salinities [28, 31-32]. The diversity of surface-liquid-gas combinations examined in the experiments is enriched by the multiplicity of contact angle measurement methods. Out of nine methodologies offered in [33], researchers commonly use the sessile drop method [34], the captive bubble method [35-36], the capillary rise method [37] and direct measurement with atomic force microscopy [38].

Experimental results have answered many questions on quantification of quartz wettability in CO_2 atmosphere with respect to the number of independent parameters such as pressure, temperature, salinity and salt type [2]. When these parameters, for example the degree of hydroxylation, are difficult or even impossible to control experimentally because of chemical side reactions or contaminations, theoretical methods complement obtained data and provide deeper theoretical understanding. There are number of studies employing computational methods to simulate wetting behaviour of water on surfaces of minerals including quartz, in particular in presence of carbon dioxide and often in the context of carbon geo-sequestration [39-51]. Theoretical studies have explored possible surface structures and predicted contact angles in CO_2 environment on pristine [41] and hydroxylated [43] surfaces, as well as the dependence of the contact angle on the degree of hydroxylation [45]. Chen [47] studied the effect of CO_2 contamination with CH_4, Ar and H_2S on the water-CO_2 interfacial tension and on the contact angle of a water droplet in CO_2 atmosphere on a silica surface. In the computational work [41] the (001) surface of α-quartz was reconstructed. In studies reported in [43, 45, 47] previously developed force field and a surface model database for silica [18] were used. In [18] the surface models were derived from the $(10\overline{1})$ plane of α-cristobalite, which is stable above 1470°C and metastable at lower temperatures, and from the (100) plane of α-quartz. In [46] the $(2\overline{0}2)$ plane of α-cristobalite was used to study how ion type and salinity affect wettability of quartz in presence of CO_2.

In practical realizations of carbon capture and storage technology, quartz surfaces are far from the studied ideal ones. Deep saline aquifers, coal beds and depleted oil or gas reservoirs are considered as possible storage media for carbon dioxide [24]. Within these formations mineral surfaces can be alkylated surfaces with chemisorpt organics [3, 52], or are almost completely composed of organic matter (coal). Experimental studies indicate that these surfaces are intermediate-wet to strongly CO_2-wet [3, 21, 29, 53]. To understand wetting of these alkylated surfaces and to explore wettability beyond the single contact angle we use fully hydroxylated (001) α-quartz surfaces with the highest theoretically possible concentration of hydroxyl groups (i.e. 9.4 OH/nm^2 [18]). Note that the concentration of OH groups on

this surface is twice the average concentration observed in nature 4.6 OH/nm^2 [19]. This surface thus has the highest theoretically possible hydrophilicity. We demonstrate that this extreme hydrophilicity can be dramatically altered (lowered) even by minute concentrations of chemisorpt organics, consistent with experimental data [3], which has serious implications for the carbon geo-storage capacity and security.

Computational Details

A general purpose parallel molecular dynamics simulation package DL_POLY 4.08 was applied to perform classical molecular mechanics computations [54-55]. Ab-initio Density Functional Theory (DFT) calculations were performed with the version 6.3 of the Quantum ESPRESSO suite of computer codes, specifically PWscf and PostProc [56-57]. The Bader charge analysis [58] was performed with the version 1.03 of "Code: Bader Charge Analysis" [59-62]. Results of the simulations were visualized with VMD [63] and VESTA [64] software, the latter package was also used for some structural manipulations. The DL_POLY Graphical User Interface was used to prepare a model C_5H_{11} group.

In all classical molecular dynamics simulations integration of the equations of motion was done with the velocity Verlet algorithm [65]. The time step in all simulations was set to 2 fs. In the NPT simulations the Nose-Hoover thermostat and barostat [66-67] with the relaxation constants 0.05 and 0.5 ps, respectively, were used. In the NVT simulations the Nose-Hoover thermostat with the relaxation constant 0.05 ps was used. Interactions cutoff distance was set to 17 A in all calculations. Electrostatics were computed with the smoothed particle mesh Ewald summation [68-69].

Force Fields

A combination of force fields was employed in this study. The quartz crystal, the hydroxylated quartz surface and the SPC water [70] were modelled with parameters of the CLAYFF force field [71]. Carbon dioxide was represented by the EPM2 model [72]. Chemisorpt pentyl groups were simulated with the DREIDING force field [73]. Ab-initio DFT calculations were used to rationalize parameters applied for coupling the CLAYFF and the DREIDING force fields, specifically the charges on atoms of the OC bond connecting the hydrocarbons to quartz.

Water and carbon dioxide molecules in all simulations, as well as the OH groups in the initial preparation of the hydroxylated quartz surface were treated as rigid bodies. Geometrical details of the rigid bodies were taken from the corresponding molecular models and force fields: CO distance (EPM2 CO_2) 1.149 A; OH distance (SPC H_2O) 1 A; HOH angle (SPC H_2O) 109.47°; OH distance (hydroxyl) 1 A. To get convenient for pentyl groups integration onto the surface orientation of the OH groups involved in the weak hydrogen bonds (pointing slightly upwards, see [11, 13]), and to highlight and isolate the weak hydrogen bonds - the place of attachment of the pentyl groups, only non-bond CLAYFF force field terms were used in the initial preparation of the hydroxylated quartz surface. All OH bond and Si-O-H angular potentials of the silanol groups were accounted for in the equilibration and the production runs of the fully assembled systems (alkylated quartz surface, water droplet, molecules of the CO_2 phase).

Parameters of potentials used to model the van der Waals interactions between all atomic species of studied in this work systems are listed in Table 1.

Table 1. Non-bond potential parameters used in the simulations [71, 73].

Atomic species	A, A^{12}·kcal/mol	B, A^6·kcal/mol	q, e	m, amu
C (CO_2)	$4.31282 \cdot 10^4$	$9.82063 \cdot 10^1$	0.6512	12.0107
O (CO_2)	$3.87857 \cdot 10^5$	$4.98236 \cdot 10^2$	-0.3256	15.9994

Atomic species	A, A^{12}·kcal/mol	B, A^6·kcal/mol	q, e	m, amu
O (H_2O)	$6.29342 \cdot 10^5$	$6.25459 \cdot 10^2$	-0.82	15.9994
H (H_2O)	0	0	0.41	1.0079
Si (SiO_2))	$1.23698 \cdot 10^1$	$9.54288 \cdot 10^{-3}$	2.1	28.0855
O (SiO_2 bridging)	$6.293422 \cdot 10^5$	$6.254591 \cdot 10^2$	-1.05	15.9994
O (SiO_2 hydroxyl)	$6.293422 \cdot 10^5$	$6.254591 \cdot 10^2$	-0.95	15.9994
H (SiO_2 hydroxyl)	0	0	0.425	1.0079
C (O-C_5H_{11})	1171341.71	667.516584	0 (0.338301)*	12.0107
H (O-C_5H_{11})	17198.6333	32.3369279	0	1.0079
O (O-C_5H_{11})	232115.998	298.083888	-0.863301**	15.9994

*charge on carbon of the OC bond is shown in brackets (estimated on basis of DFT calculations); **estimated on basis of DFT calculations.

Parameters in Table 1 correspond to the following analytical expression for the potential (U) [74]:

$$U(r) = \frac{A}{r^{12}} - \frac{B}{r^6},$$

where r is the interatomic distance.

The following formulae were used to convert original CLAYFF parameters (D_0, R_0) to parameters representing the 12-6 potential [71]:

$$A = D_0 R_0^{12},$$

$$B = 2 D_0 R_0^6.$$

The EPM2 potential parameters were converted to 12-6 potential parameters using [72]:

$$A = 4\varepsilon\sigma^{12},$$

$$B = 4\varepsilon\sigma^6.$$

The interaction parameters between unlike atoms were obtained as the geometric mean for both A and B, Lorentz-Berthelot rules [75-76]:

$$A_{ij} = \sqrt{A_i A_j},$$

$$B_{ij} = \sqrt{B_i B_j},$$

where i and j are indices of the unlike atoms.

Apart from the rigid bodies all bonds and angles were treated explicitly using bond and angle potentials. The energy of every bond stretch was described by a harmonic relationship [74]:

$$U(r_{ij}) = \frac{k_1}{2}(r_{ij} - r_0)^2,$$

where k_1 is the force constant, and r_0 represents the equilibrium bond length, see Table 2.

Table 2. Bond stretch parameters used in the simulations [71, 73].

Species i	Species j	k_1, kcal/mol/A^2	r_0, A
O (SiO_2 hydroxyl)	H (SiO_2 hydroxyl)	1108.2698	1.0
C (O-C_5H_{11})	H (O-C_5H_{11})	700.0	1.09

Species i	Species j	k_1, kcal/mol/A^2	r_0, A
C (O-C_5H_{11})	C (O-C_5H_{11})	700.0	1.53
C (O-C_5H_{11})	O (O-C_5H_{11})	700.0	1.288
Si (SiO_2)	O (O-C_5H_{11})	700.0	1.455

The Si-O-H angles (θ) of attached to the quartz surface hydroxyl groups were restrained by the harmonic potential [74]:

$$U(\theta) = \frac{k_2}{2}(\theta - \theta_0)^2,$$

where k_2 = 60.0 kcal/mol/rad^2 is the force constant, and θ_0 = 109.47° is the equilibrium bond angle [71].

Bending of the Si-O-C_5H_{11} angles of attached to the quartz surface O-C_5H_{11} groups were modelled and parametrized according to the cosine potential [74]:

$$U(\theta) = A_1(1 + \cos\theta),$$

where A_1 = 100.0 kcal/mol [73].

Bending of all intramolecular angles of the O-C_5H_{11} groups were modelled and parametrized using the harmonic cosine potential [74]:

$$U(\theta) = \frac{k_3}{2}(\cos\theta - \cos\theta_0)^2,$$

where k_3 = 112.499693 kcal/mol is the force constant, and θ_0 = 109.471° is the equilibrium bond angle [73].

Torsion of all intramolecular dihedral angles (φ) of the O-C_5H_{11} groups were modelled and parametrized according to the cosine potential [74]:

$$U(\varphi) = A_2(1 + \cos 3\varphi),$$

where A_2 = 0.11111111 kcal/mol [73].

Modelling of the Oxygen-Carbon Bond

Utilized in this work force fields are designed and well suited for modelling minerals (the CLAYFF force field [71]) and for modelling of organic molecules (the DREIDING force field [73]). However, specific for the purpose of this study description of a polar OC bond connecting pentyl groups to the quartz surface is not provided by either the CLAYFF or the DREIDING force fields. Thus, to extend capabilities of the force field pair a physically reasonable estimation of charges on oxygen and carbon atoms of the OC bond is necessary. This estimation was obtained from the DFT calculations which were performed as follows. Out of the orthorhombic cell of quartz crystal [77] a super cell 2x1x1 was constructed (overall 36 atoms, 12 silicon atoms and 24 oxygen atoms). Using this cell three stages of computations were then performed. In the first stage the lattice vectors of the crystal were allowed to be changed and optimized during relaxation of ionic positions of the cell. In the second stage a three-layer slab (three heights of the orthorhombic cell) was constructed with a fully hydroxylated surface and integrated pentyl group, 30 A of vacuum space was provided above the surface, see Figure 1. Only ions of this system were then relaxed with atoms of the bottom layer (one height of the orthorhombic unit cell) of the slab being fixed. In the third stage distribution of the charge density of the relaxed slab was determined with a single point energy calculation. In the third stage of these computations the kinetic energy cutoffs for plane waves and for charge density were set to 40 and 1500 Ry, respectively. The first Brillouin zone in the reciprocal space was sampled with the Monkhorst-Pack mesh [78] 5x5x1. We

used the PAW (Projector Augmented Wave method) [79] potentials H.pbe-kjpaw_psl.0.1.UPF, C.pbe-n-kjpaw_psl.0.1.UPF, O.pbe-n-kjpaw_psl.0.1.UPF and Si.pbe-n-kjpaw_psl.0.1.UPF from [80]. The electron exchange and correlation energy was approximated by the PBE (Perdew, Burke and Ernzerhof) functional [81].

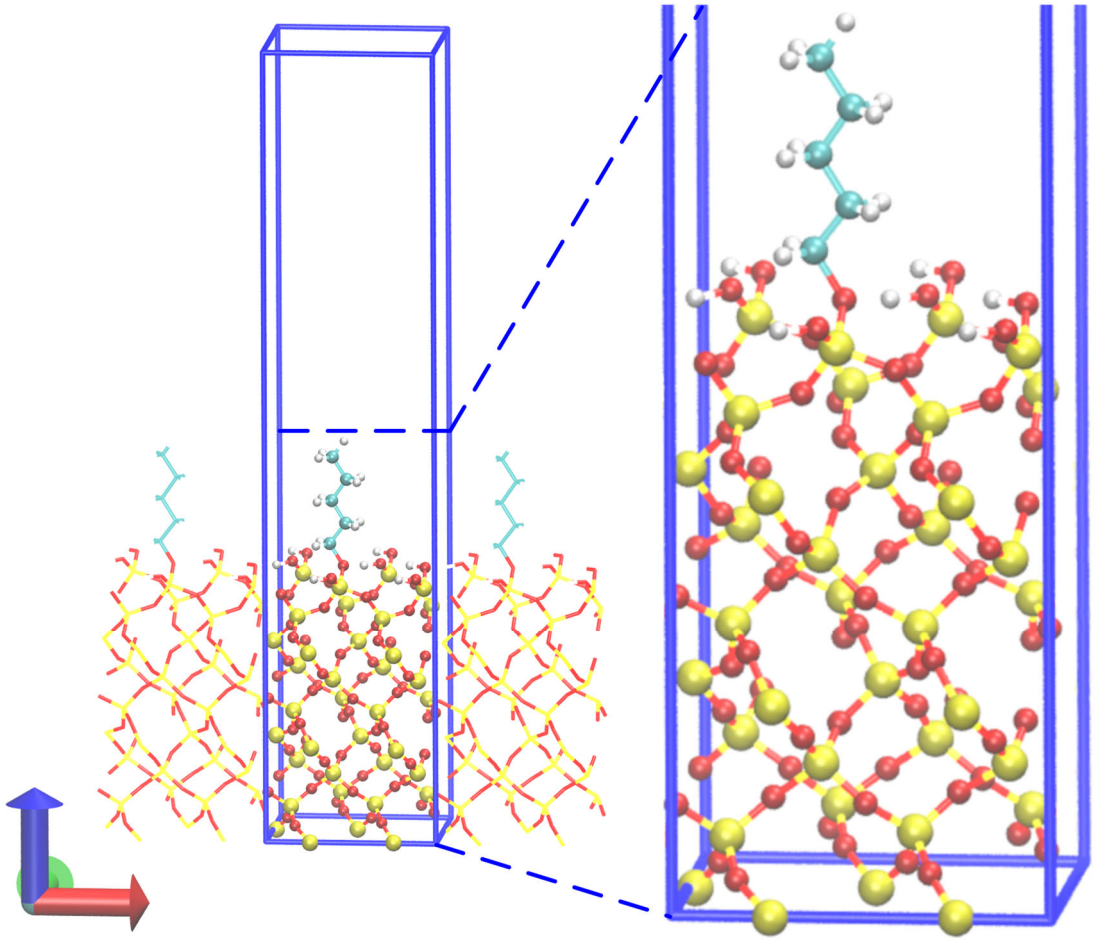

Figure 1. Optimized at the DFT level of theory three-layer quartz slab with integrated pentyl group. White balls - hydrogen atoms, light blue balls - carbon atoms, red balls - oxygen atoms, yellow balls - silicon atoms. Blue lines demark the unit cell of the simulated system, images of which are shown with lines instead of the balls.

The Bader charge analysis performed on the DFT computed electronic density resulted in a charge of -1.311489 e on the oxygen atom, and a charge of 0.338301 e on the carbon atom. This positive carbon charge corresponds to 0.796 of the charge on the hydroxyl hydrogen of the CLAYFF force field (the hydrogen atom which is to be removed and replaced by the carbon atom of the pentyl group). We assign this fraction of the CLAYFF hydroxyl hydrogen charge to the carbon of the OC bond. The rest of the hydroxyl hydrogen charge assigned to the oxygen of the OC bond makes the atom approximately 90% as negative (-0.863301 e) as the hydroxyl oxygen (-0.95 e) of the CLAYFF force field. This 90% proportion aligns well with results of the Bader charge analysis where the charges on these two oxygen atoms of the same geminal silanol group are -1.311489 and -1.477656 e, respectively. With these operations we thus resolve two problems at the same time. We replace the hydroxyl hydrogen with carbon of the pentyl group, and we redistribute the charge of the replaced hydrogen atom between the carbon and the oxygen atoms of the OC bond in a manner consistent with the DFT results.

Preparation of Alkylated Quartz Surfaces

Construction and modelling of modified (contaminated with hydrocarbons) quartz surfaces is hampered by the fact that structures of surfaces of pure quartz polymorphs are not well characterised even in 2018 [16-17]. On the basis of previous reconstructions of the hydroxylated (001) α-quartz surface [11-13] we suggest several model quartz surfaces with integrated pentyl groups. These models are then used to quantify the effect of quartz surface contamination with hydrocarbons on its wettability.

Preparation of the modified surfaces proceeded as follows: out of the primitive unit cell of α-quartz [82] its orthorhombic cell was created according to [77]. The latter cell was then used to construct a super cell 2x1x1 (overall 36 atoms, 12 silicon atoms and 24 oxygen atoms). Out of this cell a super cell 4x5x8 was created to equilibrate the crystal at 1 atm pressure and 300 K temperature over 10^5 steps. The system was simulated in the NPT ensemble. Used throughout this study, lattice vectors of the equilibrated orthorhombic super cell 2x1x1 amounted to the following values 9.989x8.651x5.492 A, only 1.6% larger than the crystallographic values obtained from [82]. Four of these 2x1x1 cells (two in x direction and two in y direction) were then used to prepare a unit cell of fully hydroxylated quartz slab. The unit cell of the top layer of the 5x6x4 slab is shown in Figure 2. To obtain an ordered surface structure this four-layer (a layer in terms of the unit cell height) slab was relaxed at 10 K for 10^5 steps. The system was simulated in the NVT ensemble. Atoms of the lowest laying layer (one unit cell height) of the slab were fixed to emulate the bulk crystal.

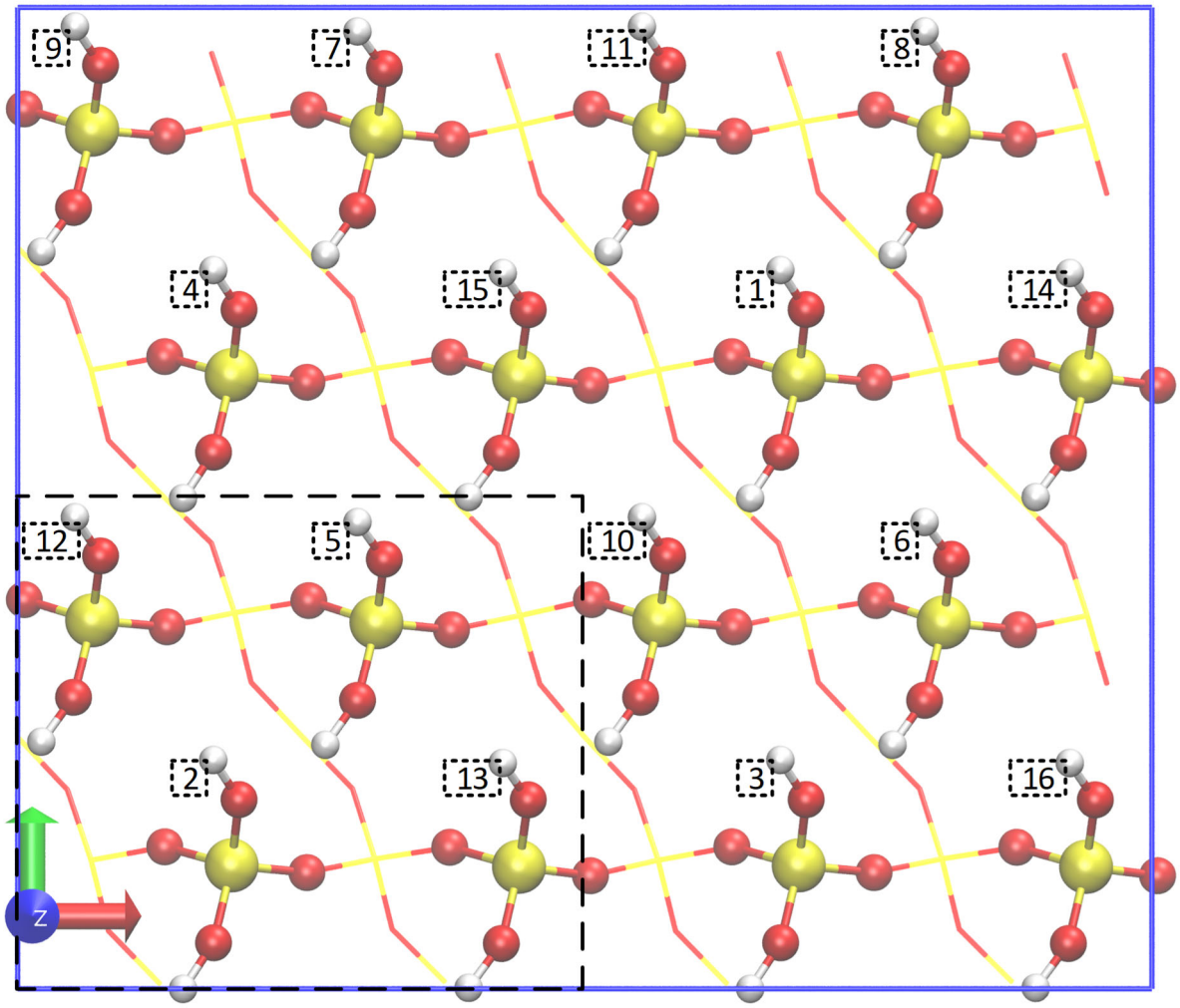

Figure 2. Top view of the unit cell of the top layer of the fully hydroxylated quartz surface. White balls - hydrogen atoms, red balls - oxygen atoms, yellow balls - silicon atoms. Top SiO_4H_2 groups are shown with balls, lower atoms are shown with lines of the same colour. Dashed parallelogram demarks the 2x1x1 super cell of the orthorhombic unit cell. Numbers illustrate the cumulative alkylation sequence.

To explore the influence of different alkyl group surface concentrations on the contact angle, a uniform alkylation of the hydroxylated quartz surface was applied according to the cumulative sequence illustrated in Figure 2. The hydrogen atom of the geminal silanol group, which is not involved in formation of the strong hydrogen bond [11-13], was replaced with a pentyl (C_5H_{11}) group. The resulting 16 surfaces with C_5H_{11} surface concentrations ranging from 0.29 to 4.63 groups/nm^2 (in 0.29 groups/nm^2 steps) are demonstrated in Figure 3. The fully pentylated surface is depicted in Figure 4.

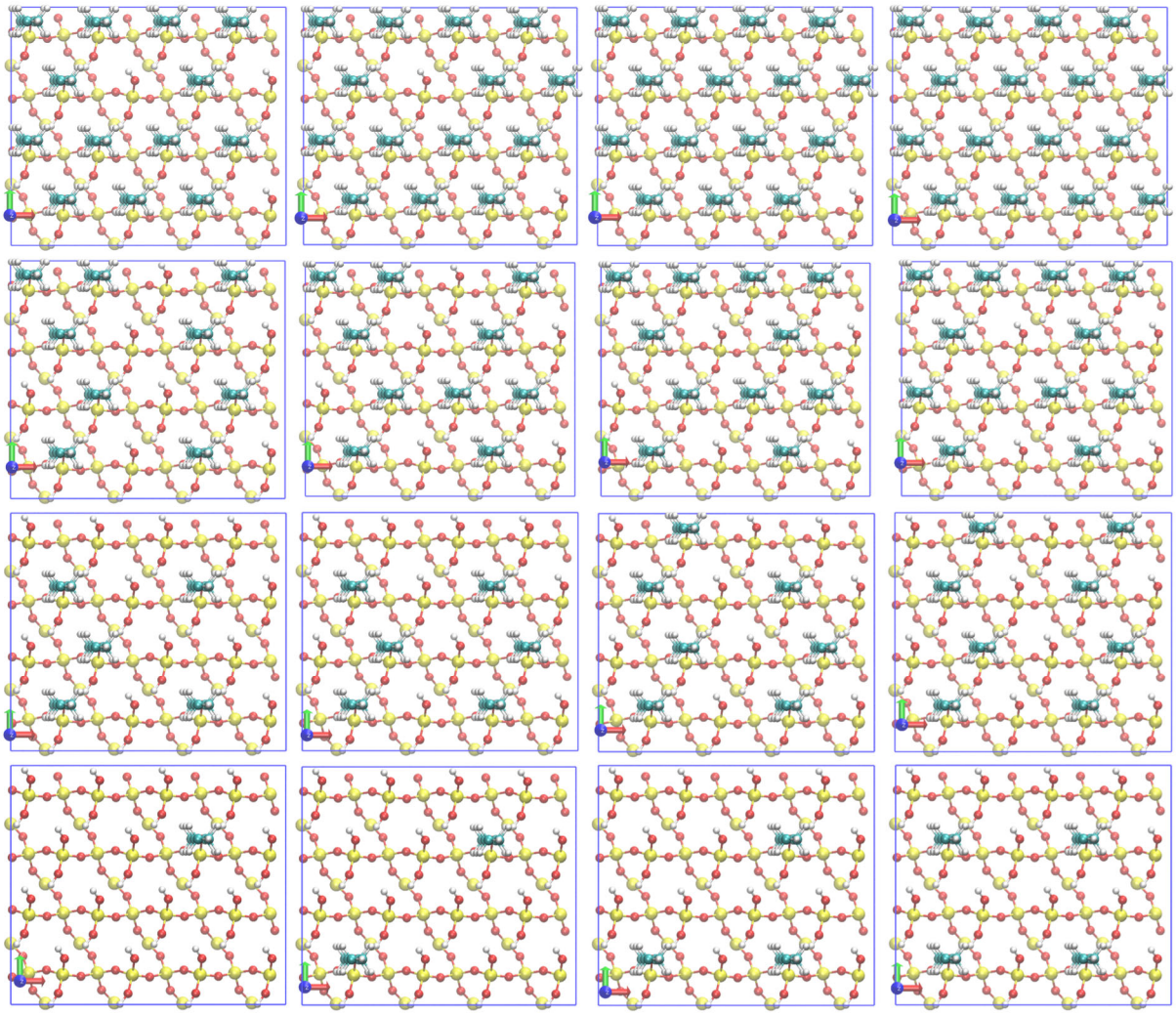

Figure 3. Top views of the top layer unit cells. 16 quartz surfaces with surface pentyl concentrations ranging from 0.289 to 4.629 groups/nm^2 (surfaces 1 to 16) are shown, unit cells are ordered from left to right and from bottom to top. White balls - hydrogen atoms, red balls - oxygen atoms, light blue balls - carbon atoms, yellow balls - silicon atoms.

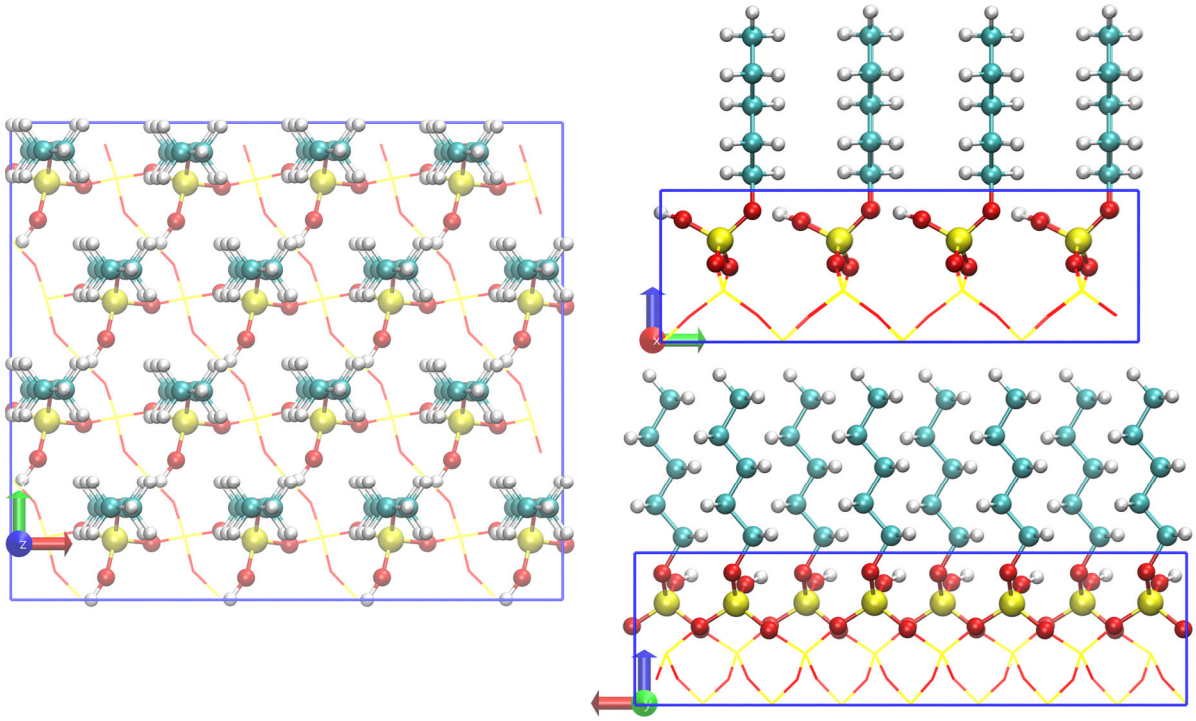

Figure 4. Top view (left) and views along x (right top) and y (right bottom) directions of fully pentylated quartz surface (surface 16). White balls - hydrogen atoms, red balls - oxygen atoms, light blue balls - carbon atoms, yellow balls - silicon atoms. Top $SiO_4HC_5H_{11}$ groups are shown with balls, lower atoms are shown with lines of the same colour. Only top layer unit cell of four-layer slab is demonstrated.

It is worth noting that even a fully pentylated quartz surface still has a very high concentration of hydroxyl groups. Thus, with an increase in pentyl group concentration from 0 to 4.63 groups/nm^2 the concentration of hydroxyl groups simultaneously decreases linearly from 9.26 to 4.63 groups/nm^2, see the supporting information.

Simulation Setups

Using these alkylated quartz surfaces, 16 models overall containing a water droplet and CO_2 gas were prepared. Simulations were performed at 300 K and 10 MPa CO_2 pressure. The number of CO_2 molecules corresponding to this PT-condition in every simulation box was determined according to [83] and amounted to 7188, 7137, 7086, 7035, 6984, 6933, 6881, 6830, 6779, 6728, 6677, 6625, 6574, 6523, 6472, 6421 for surfaces 1 through 16, respectively. When estimating the space available for CO_2 in the simulation boxes, gas volumes of the system with hydroxylated surface (no hydrocarbons) and of the system with fully pentylated surface were calculated as free space from the surface up to the CO_2 constraining potential. The volume of the water droplet was subtracted from the latter values, see Figure 5. The space available for CO_2 for the systems with intermediate pentyl group concentrations were obtained by interpolation.

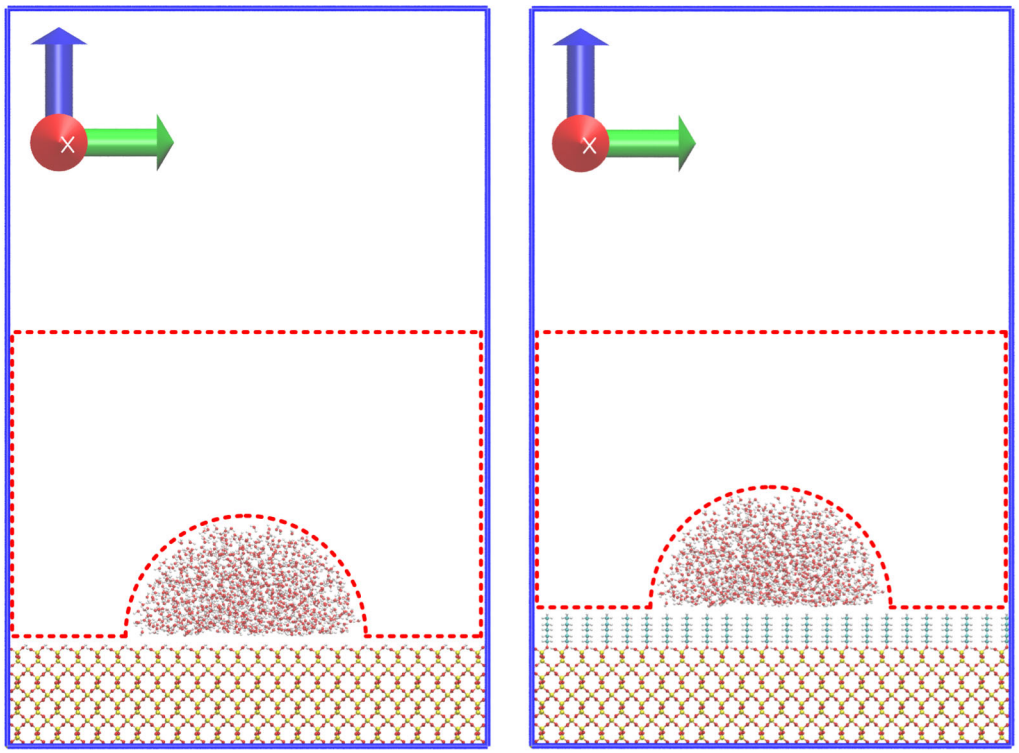

Figure 5. Space available to CO_2 in the hydroxylated (left) and fully pentylated (right) systems. Dashed red line demarks volume available to CO_2. White balls - hydrogen atoms, red balls - oxygen atoms, light blue balls - carbon atoms, yellow balls - silicon atoms.

Uniformly distributed carbon dioxide and water molecules were pre-equilibrated at 300 K in 100x104x60 and in 50x50x50 A boxes, respectively. Water density was taken to be 1000 kg/m^3. Dynamics of these two systems were modelled in the NVT ensemble. Overall $5 \cdot 10^5$ steps were performed for CO_2 and 10^5 steps for H_2O.

A half sphere of radius 26 A atop of the C_5H_{11} groups was filled with water molecules from the above described box. 946 H_2O molecules fit into the "water droplet". These "water droplets" were placed in the centre of the slabs. The rest of the space up to 60 A above the C_5H_{11} groups was filled with pre-equilibrated carbon dioxide. Vacuum space of 70 A was provided on top of the 60 A above the C_5H_{11} groups. All simulations were performed with periodic boundary conditions in x and y directions. In z direction a repulsive force was set at 60 A above the tip level of C_5H_{11} groups:

$$F = k(z_0 - z), z > z_0,$$

where k=1 kcal/mol - is the force constant, and z_0 is the position of the repulsive potential.

The distance to the repulsive potential (60 A above the C_5H_{11} groups) ensures that the contact angle at the surface is not affected by perturbations in the CO_2 density caused by the wall.

Dynamics of the quartz-C_5H_{11}-H_2O-CO_2 systems were then simulated in the NVT ensemble. Overall $1.5 \cdot 10^6$ production steps (3 ns simulation time) were performed for every system preceded by $3 \cdot 10^5$ equilibration steps. Atoms of the lowest laying layer (one unit cell height) of the four-layer quartz slab were fixed in all simulations to emulate the bulk crystal. Dimensions of the simulation boxes were 99.89x103.81x159.17 A. Figure 6 demonstrates the initial simulation setup for the surface with 1.16 C_5H_{12}/nm^2 surface concentration (four C_5H_{11} groups in the unit cell, surface 4).

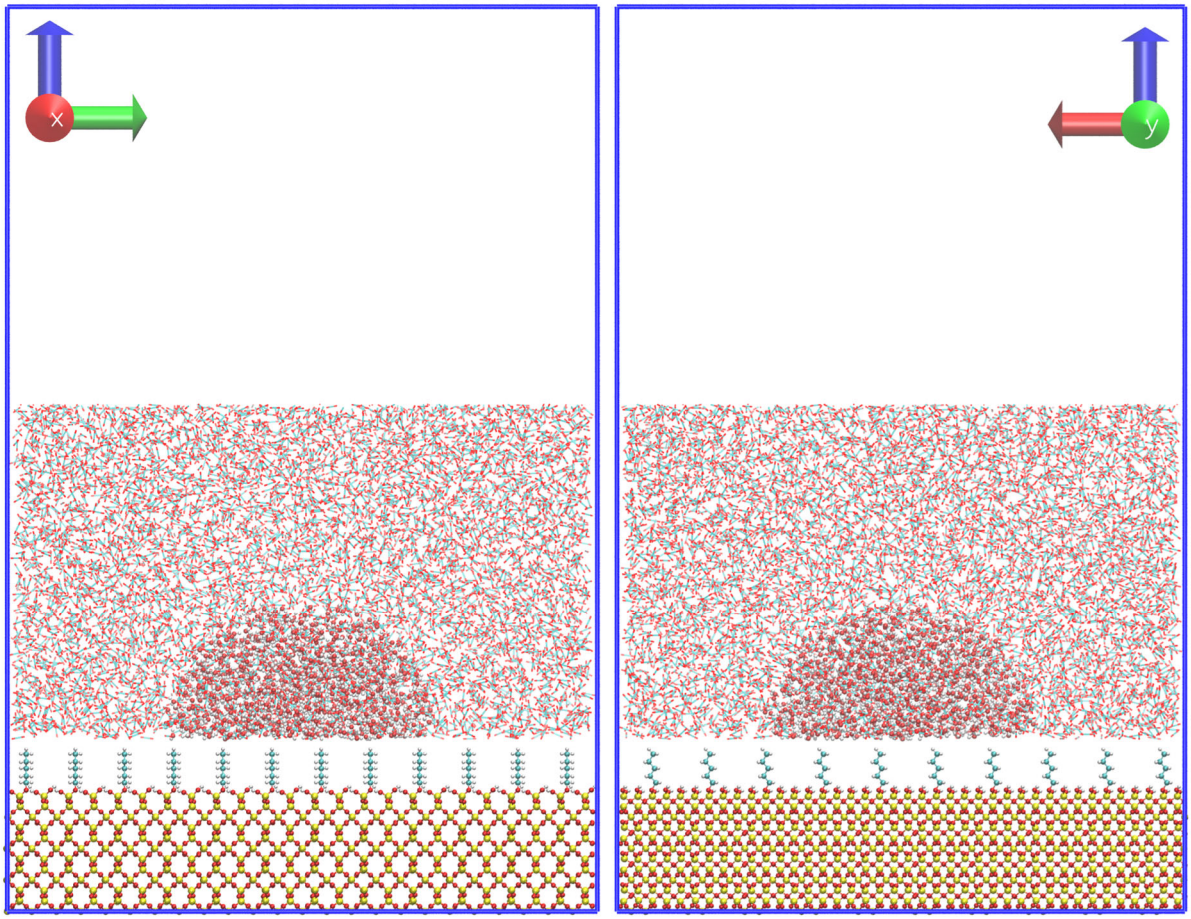

Figure 6. Initial simulation setup for the quartz surface with four C_5H_{11} groups in the unit cell (surface 4). Views along x (left) and y (right) axis. White balls - hydrogen atoms, red balls - oxygen atoms, light blue balls - carbon atoms, yellow balls - silicon atoms. To make the water droplet more visible CO_2 molecules are shown with lines.

Determination of the Contact Angle

After the production runs an additional $5 \cdot 10^4$ simulation steps were performed at the same conditions. Five simulation snapshots separated by 10^4 steps were taken from these final runs for the analysis. The contact angle was calculated using the water iso-density charts. To construct the charts the axis of a sufficiently large cylinder was aligned with the vertical axis passing through the centre of mass of all water molecules of a snapshot. The cylinder was then divided into thin disks dH, see Figure 7. Starting from the maximum radius Rmax and proceeding towards the central vertical axis, water density in every ring dR of thickness dH was calculated and compared with the half of water normal density (i.e. 0.033/2 water molecules per cubic angstrom). In every disk a position (H+dH/2, R+dR/2), where the water density first exceeds, if it exceeds at all, the half of the normal water density was recorded as the point of the iso-density.

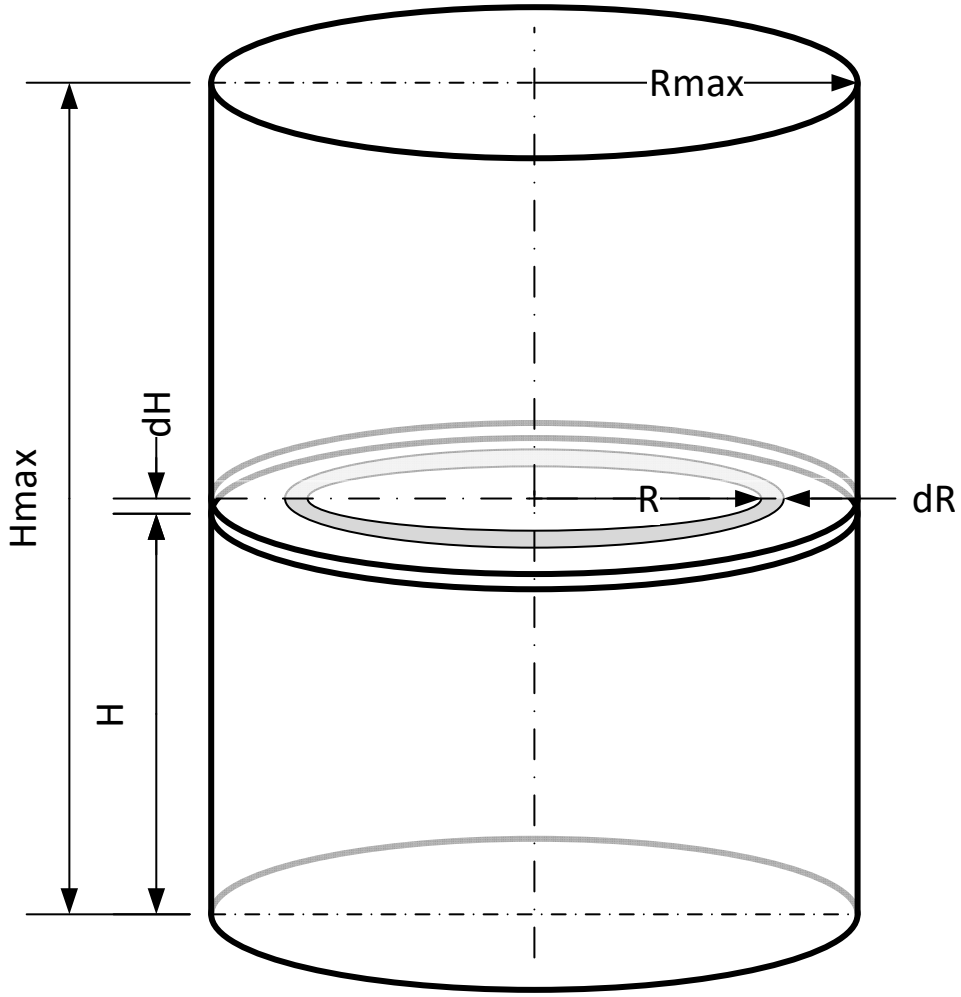

Figure 7. Schematic illustration of calculations of the water iso-density.

The choice of dH and dR is a trade-off between two factors. Very small values result in only few molecules present within the ring's volume, which is also too small. The small number in the denominator in the density calculations in turn results in data scattering and significant errors. Very large values on the other hand smooth the density too much, which removes details and reduces accuracy. The following protocol was applied to substantiate the used values. Starting with 0.25 A for the dH and dR they were then increased one after another in 0.25 A steps until the algorithm became insensitive to molecules which escaped to the gas phase from the water droplet. Thus dH and dR amounted to 1.5 and 1.25 A, respectively.

Constructed in the described way iso-density charts were then used to find the radius and position of a circle which best approximates the iso-density. The circle's position was limited to the vertical axis of the iso-density plot, which is the vertical axis passing through the centre of mass of all water molecules of the simulation snapshot. The BFGS algorithm [84-87] was applied to find the minimum of a sum of absolute differences between the data points and the circle's profile. The theoretical and the apparent contact angles (for the definitions see the qualitative analysis of the results below) were then calculated as the angles of the tangential line to the circle's contour at its interception point with the surface. The quartz surface was set at the average vertical position of the hydrogen atoms of the hydroxyl groups, and the tip level of the pentyl groups was found as the average position of the top three hydrogen atoms of all C_5H_{11} groups in the snapshot. Averaged over the five simulation snapshots iso-density charts were used to calculate the hidden contact angle.

Results and Discussion

Qualitative Analysis of the Results

As an example, water iso-density chart with close to the average parameters (the contact angle, radius and vertical position of the spherical water droplet) and the circle fitted to the data points for quartz surface with pentyl concentration 1.157 C_5H_{11}/nm^2 (surfaces 4) is shown in Figure 8. The same iso-density charts for quartz surfaces with pentyl concentrations 0.289 through 3.182 groups/nm^2 (surfaces 1 through 11) are collected in the supporting information. All averaged contours of the water droplets for surfaces 1-11 gathered in one image are shown in Figure 9.

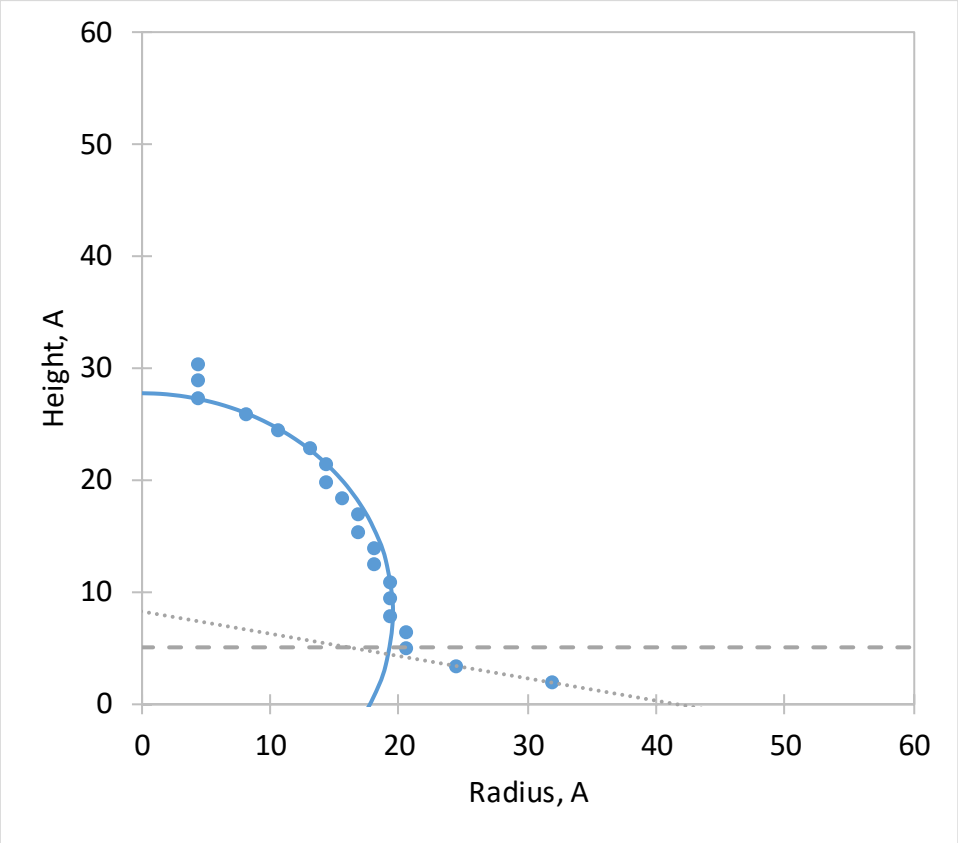

Figure 8. Water iso-density chart for quartz surface (surface 4) with concentration of pentyl groups 1.157 C_5H_{11} per square nm. The iso-density data points are shown with blue dots, fitted circle is shown with blue line, the tip level of the pentyl groups is shown with the dashed line, the dotted line illustrates the planar projection of the water "skirt".

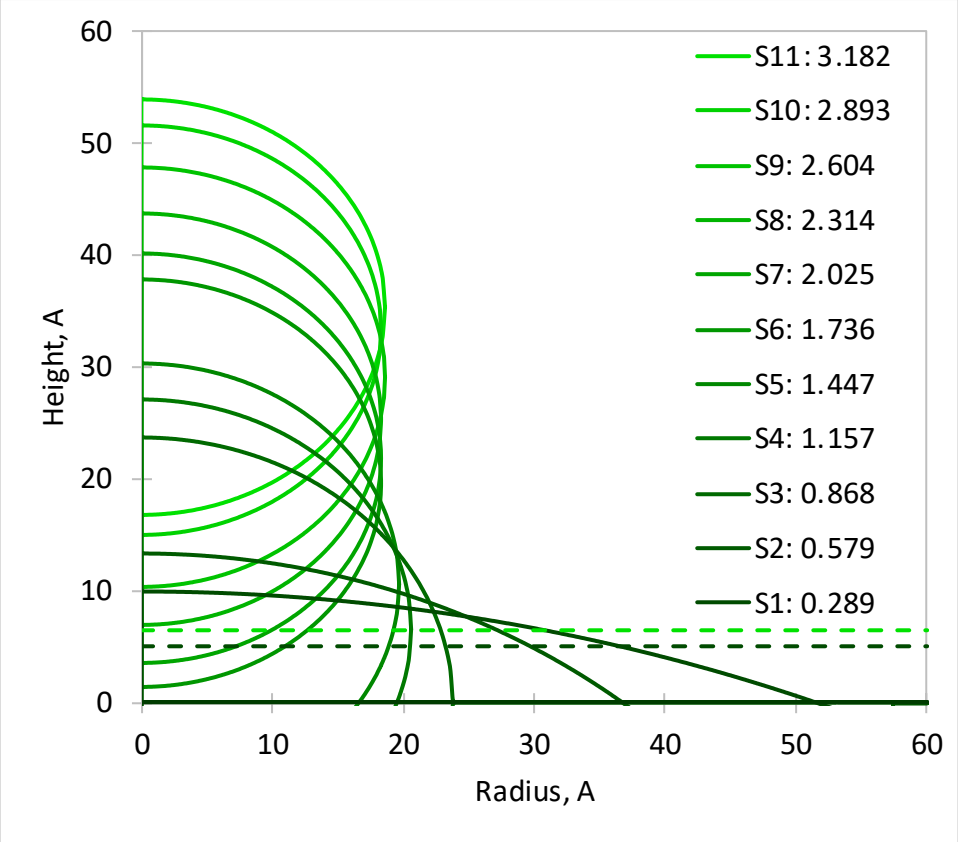

Figure 9. Averaged contours of water droplets for surfaces 1 (S1) through 11 (S11) with corresponding concentrations of pentyl groups per square nm (ascending water droplet). Dashed horizontal lines represent the lowest and the highest tip levels of the pentyl groups.

Examination of the water iso-density contours in the supporting information and Figure 9 reveals that the spherical water droplet losses contact with the quartz surface and the tip level of the pentyl groups when their concentration is higher than 2.604 C_5H_{11} per square nm. The surface 10 does not have any connection with the droplet at all, even via a "tail" of water molecules. These observations drawn from the iso-densities are also supported by visual inspection of corresponding simulation snapshots with removed CO_2 molecules shown in the supporting information and exemplified here for the surface 10 in Figure 10. Above a 2.893 groups/nm^2 pentyl surface concentration (surface 10), the water droplet floats freely in the CO_2 phase. For concentrations higher than 3.182 groups/nm^2 (surface number higher than 11), the dimensions of the simulation box become too small for the droplets' motion and its distance travelled over the simulation period, the droplets interact with the repulsive wall, and cross borders of the simulation box.

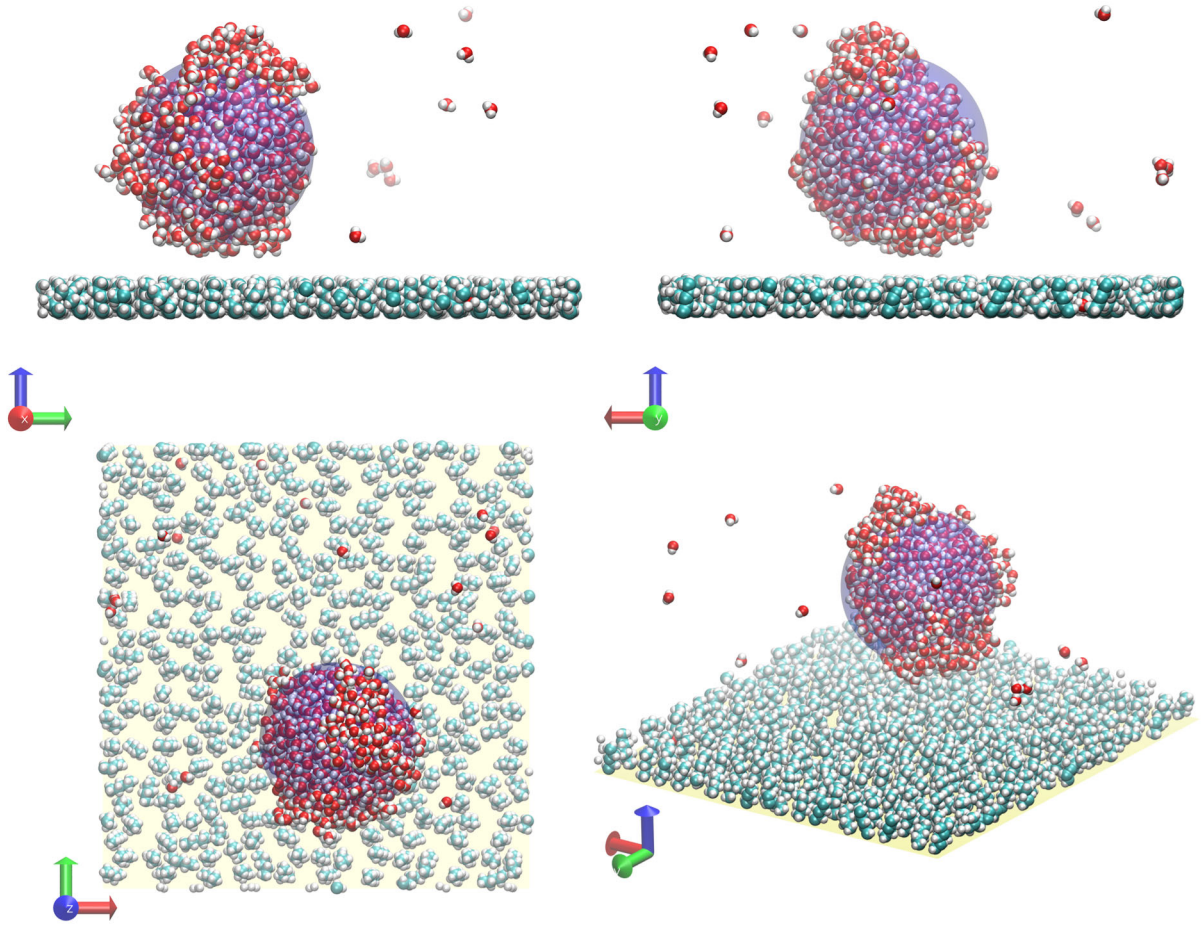

Figure 10. Simulation snapshot of the quartz surface with pentyl concentration 2.893 groups per square nm (surface 10). View along x axis: top left; view along y axis: top right; view along z axis: bottom left; isometric view: bottom right. The sphere fitted to the iso-density chart is illustrated in light purple color. The surface is illustrated with square in light yellow color. Water molecules and pentyl groups are shown in VDW representation, white balls - hydrogen atoms, red balls - oxygen atoms, light blue balls - carbon atoms.

Additionally, the water iso-density charts indicate that a water "skirt" is formed between the quartz surface and the tip level of the pentyl groups. The water "skirt" is envisaged by authors as a conical frustum or a truncated cone. In the iso-density chart in Figure 8, and in the charts provided in the supporting information, planar projections of the "skirts" are shown with the dotted lines. These lines represent the fits to the first closest to the quartz surface peak in the water iso-density and the next highest data point of the iso-density. Formation of the "skirt" can also be supported by a simple visual examination of the side views of corresponding simulation snapshots with removed CO_2 molecules and C_5H_{11} groups, see Figure 11 and the supporting information. The "skirt" is particularly clearly visible in the snapshot for the surface 4, view along y axis; in the snapshot for the surface 5, view along x axis; in the snapshot for the surface 6, view along y axis; in the snapshot for the surface 7, view along x axis; in the snapshot for the surface 8, view along x axis; in the snapshot for the surface 9, view along x axis. At low pentyl concentration, surface 1, the planar projection of the "skirt" is almost a tangential line to the droplet's profile. With increasing pentyl group concentration, the planar projection of the "skirt" starts to intersect the droplet's profile more explicitly, surface 2 and following. With further increase in concentration of C_5H_{11} groups radius of the "skirt" decreases, and the "skirt" is pulled towards the centre of the rising droplet, surfaces 8 and 9.

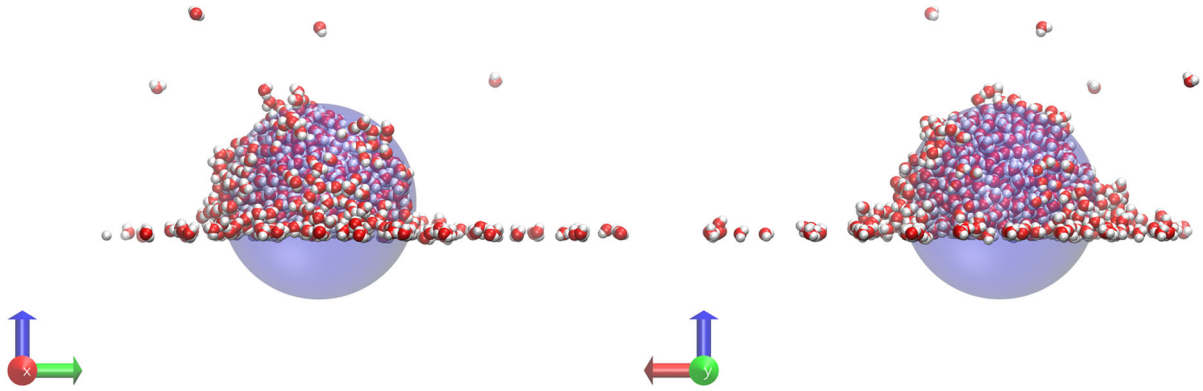

Figure 11. Side views of a water droplet on the quartz surface with removed pentyl groups for pentyl concentration 1.157 groups per square nm (surface 4). View along x axis: left; view along y axis: right. The sphere fitted to the iso-density chart is illustrated in light purple color. The surface position is indicated by the lowest laying water molecules. Water molecules are shown in VDW representation, white balls - hydrogen atoms, red balls - oxygen atoms.

This qualitative review, observations and inspections of the simulation results demonstrate that the wettability of alkylated quartz surface is a complex phenomenon. There are at least two planes (levels) which can be called surfaces: the surface of quartz itself and the tip level of pentyl groups; position of the latter also depends on the concentration of C_5H_{11} groups. There is also a water "skirt" which is formed in between these two planes (levels).

To account for mentioned effects in quantitative description of the wettability of alkylated quartz surfaces we introduce the following parameters, see Figure 12. The theoretical contact angle (θ_T), the contact angle of a spherical water droplet (spherical cap) at the level of quartz surface. The apparent contact angle (θ_A), the contact angle of a spherical water droplet (spherical cap) at the tip level of pentyl groups; this contact angle is most likely to be measured in an experiment, with the difference between θ_T and θ_A being large and more noticeable for longer alkyl groups. The hidden contact angle (θ_H), the contact angle of a water "skirt" at the level of the quartz surface.

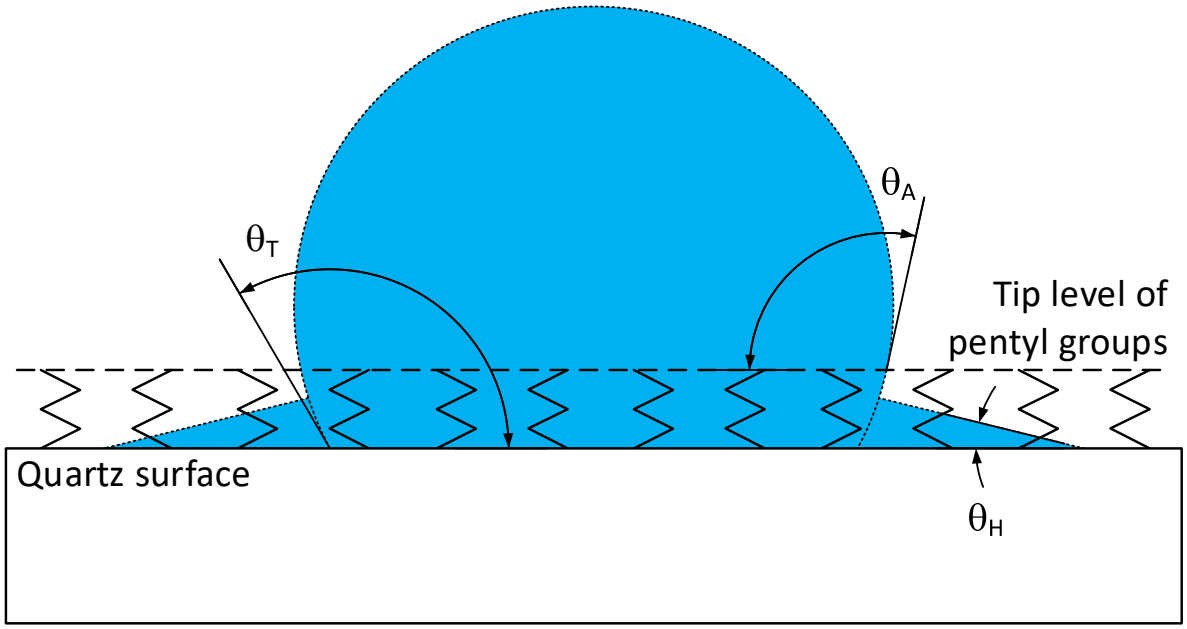

Figure 12. Parameters used to quantify the wettability of alkylated quartz surface. Water droplet and its "skirt" are shown in blue, C_5H_{11} groups are illustrated with zigzags.

Quantitative Analysis of the Results

Circles fitted to the iso-density charts and corresponding circumscribed spheres shrink with increasing pentyl group concentration. When the pentyl concentration exceeds 1.5 C_5H_{11}/nm^2 (surface number 6 and higher) the radius stabilizes at 18.4 A, see Figure 13. At this point almost all water molecules become part of a spherical droplet.

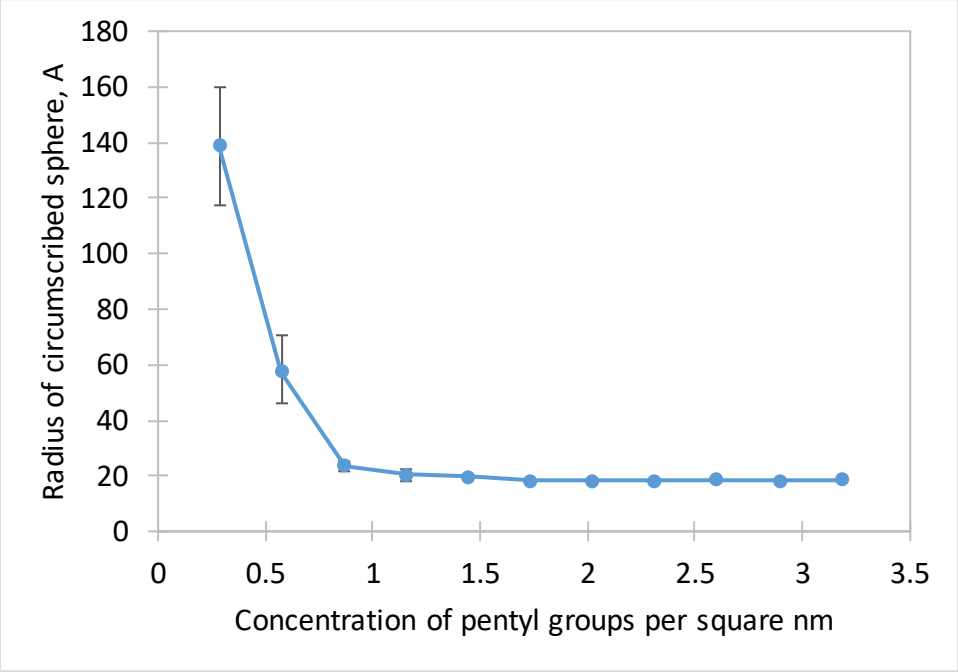

Figure 13. Dependence of the circumscribed sphere (circle) radius on concentration of pentyl groups.

With increasing pentyl concentration the droplet moves upwards, see Figure 14, and loses contact with the tip level of pentyl groups at 2.604 C_5H_{11}/nm^2 (surface 9), see Figure 15, although the water "skirt" is still present at this concentration, see the supporting information, but disappears at 2.893 C_5H_{11}/nm^2 (surface 10). Spherical part of the droplet loses contact with the quartz surface at 2.025 C_5H_{11}/nm^2 pentyl surface concentration (surface 7), see Figure 15. At this pentyl concentration the "skirt" is still in place.

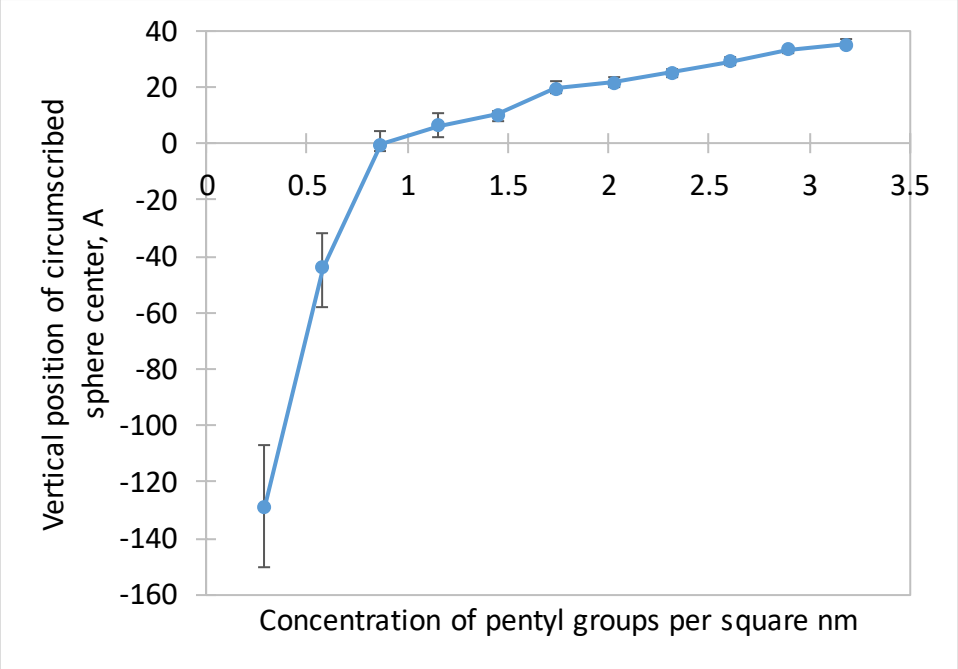

Figure 14. Dependence of the vertical position of the circumscribed sphere (circle) centre on concentration of pentyl groups. Position of the quartz surface is at zero.

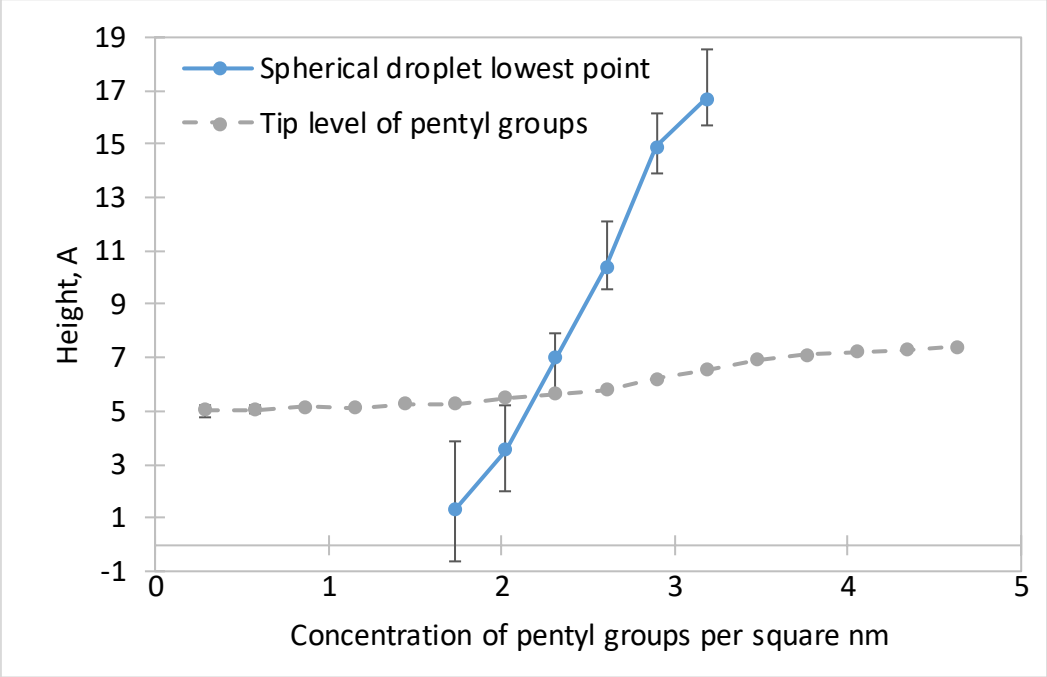

Figure 15. Circumscribed sphere (circle) or spherical droplet contact with the quartz surface (height zero) and the tip level of pentyl groups as a function of C_5H_{11} concentration.

Dependences of the theoretical and the apparent contact angles on surface pentyl group concentration are shown in Figure 16 and Figure 17, respectively. Both contact angles increase with rising pentyl concentration, while the apparent contact angle is generally smaller and increases less sharply. It is reasonable to expect that for longer alkyl groups the difference between the theoretical and the apparent contact angles will be higher because of higher tip level of the alkyl groups.

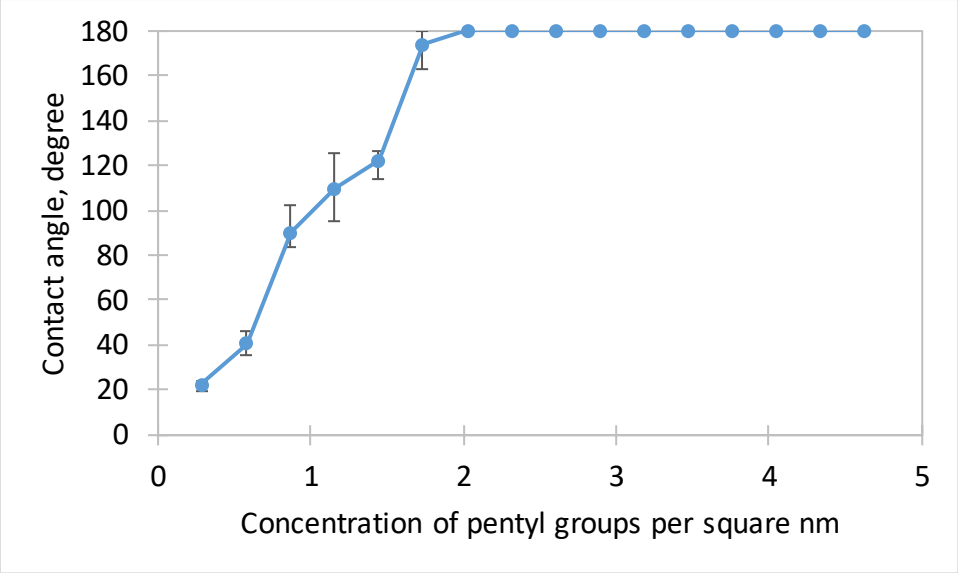

Figure 16. Dependence of the theoretical contact angle on concentration of pentyl groups.

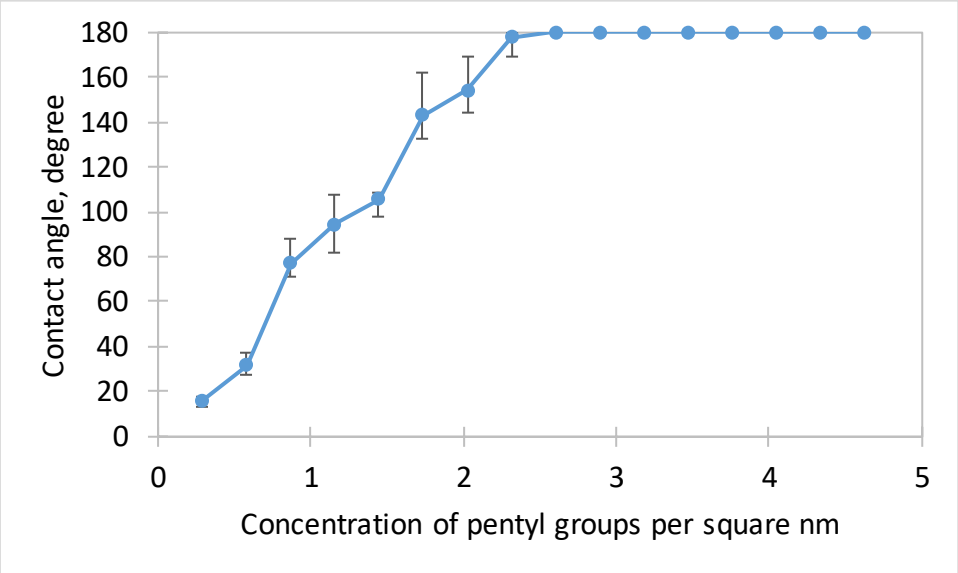

Figure 17. Dependence of the apparent contact angle on concentration of pentyl groups.

Four wettability zones can be identified in Figure 16 and Figure 17, see Table 3. The first one is the water-wet zone, where pentyl concentrations range from 0.289 to 0.579 C_5H_{11}/nm^2, surfaces 1 and 2. The second zone is intermediate-wet, where pentyl concentrations range from 0.868 to 1.447 C_5H_{11}/nm^2, surfaces 3, 4 and 5. The third zone is CO_2-wet, where pentyl concentrations range from 1.736 to 2.314 C_5H_{11}/nm^2, surfaces 6, 7 and 8.

For higher concentrations in the zone four, starting from 2.604 C_5H_{11}/nm^2, surface 9, the surfaces are completely hydrophobic (the contact angle is 180°) according to both the theoretical and the apparent contact angles.

Table 3. Wettability zones according to the theoretical and the apparent contact angles.

	Zone 1	Zone 2	Zone 3	Zone 4
Wettability	Water wet	Intermediate wet	CO_2 wet	Extremely hydrophobic

	Zone 1	Zone 2	Zone 3	Zone 4
Pentyl concentration, groups/nm^2	0.289-0.579	0.868-1.447	1.736-2.314	2.604 and higher
Surface, number	1-2	3-5	6-8	9 and higher
Theoretical contact angle, degree	22.01-40.33	89.90-122.37	173.98-180	180
Apparent contact angle, degree	15.40-31.54	77.30-105.49	143.13-177.88	180

The numerical values of the theoretical and apparent contact angles predicted here follow the same trend as observed experimentally in comparable systems obtained for calcite surfaces exposed to stearic acid, where a calcite surface was aged in highly diluted stearic acid solutions (concentrations ranged from 10^{-10} to 10^{-2}M) [3]. For these concentrations, the contact angle of a water droplet in CO_2 atmosphere measured at 10 MPa and 323 K increased from 43 to 126°. The same trend is observed in this study, where the contact angle rapidly increased in the range of small pentyl concentrations (0.289-2.314 C_5H_{11}/nm^2) from 15 to 180°.

An elaborate analysis of the hidden contact angle reveals an even more detailed picture of the processes occurring on the quartz surface. The hidden contact angle clearly demonstrates that surface 9 and the corresponding pentyl concentration (2.604 C_5H_{11}/nm^2) represent a transition concentration at which hydrophobicity takes over, see Figure 18. All surfaces with pentyl concentrations 2.893 C_5H_{11}/nm^2 or higher (surface number 10 or higher), have less affinity to water. Indeed, surface 10 is the surface where the water "skirt" disappears completely, see Figure 10.

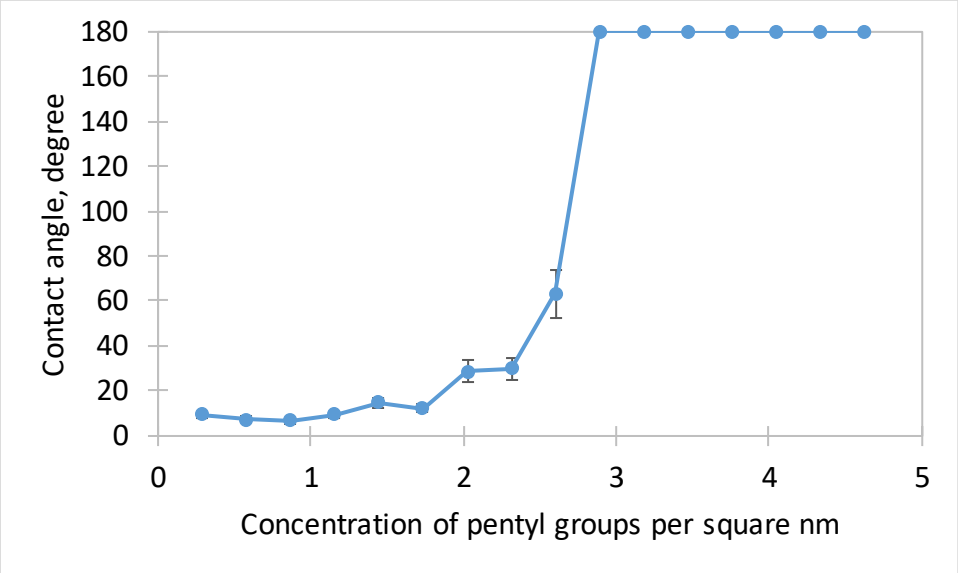

Figure 18. Dependence of the hidden contact angle on concentration of pentyl groups.

With increasing surface pentyl group concentration the hidden contact angle behaves differently in comparison with the theoretical and the apparent contact angles. Noticeable increase in the value of the hidden contact angle is observed at concentrations higher than 2 C_5H_{11}/nm^2. At concentrations 2.025 and 2.314 C_5H_{11}/nm^2 (surfaces 7 and 8) the hidden contact angle is almost 30°. It increases further to slightly more than 60° at 2.604 C_5H_{11}/nm^2 concentration (surface 9). Interestingly, the value of the hidden contact angle at a concentration of 1.736 C_5H_{11}/nm^2 (surface 6) and lower is almost constant and on average amounts to slightly less than 10°.

The hidden contact angle is thus a useful characteristic which shows that the alkylated quartz surface exhibits close to a binary behaviour in terms of its wettability. It is water wet and hydrophilic when concentrations of pentyl groups are less than 2.604 C_5H_{11}/nm^2 (surface 9), and it is extremely hydrophobic at higher pentyl concentrations, Figure 18. Very sharp rise of the contact angle over a small range of pentyl concentrations practically makes the surface either hydrophilic or hydrophobic. We attribute this close to the binary wettability to the steric effects preventing water molecules from reaching the quartz surface, compare number of water molecules at the surface 9 (and lower) and at the surface 10 (and higher) in the supporting information.

In addition to determined contact angles, it is possible to estimate when the wettability regime of alkylated quartz surfaces changes from homogenous to the heterogeneous. To do so let us first consider the basic equation of the Cassie-Baxter model [88]:

$$cos\theta_{CB} = f_1 cos\theta_1 + f_2 cos\theta_2,$$

where θ_{CB} is the Cassie-Baxter contact angle; f_1 and f_2 are the area fractions for surface components 1 and 2, for which the contact angles are θ_1 and θ_2, respectively.

The first surface component in our case is the fully hydroxylated quartz surface for which we approximate the contact angle with the average hidden contact angle (9.81°) at low pentyl concentrations 1.736 C_5H_{11}/nm^2 (surface 6) and smaller. The second surface component is the alkylated quartz surface with minimal pentyl concentration for which the contact angle becomes equal to 180°. The Cassie-Baxter contact angle is the apparent contact angle characterised in this work. Taking into account the relationship between the area fractions (f_2=1-f_1), the following expression can then be obtained:

$$f_1 = \frac{cos\theta_A + 1}{cos\theta_1 + 1}.$$

Using the last formula we calculate the surface area per one C_5H_{11} group and plot it as a function of C_5H_{11} concentration, Figure 19. At concentrations 0.868 C_5H_{11}/nm^2 (surface 3) and higher, the surface area per one pentyl group stabilizes at 0.46 nm^2 per group. The concentration at which this surface area becomes constant is the concentration when the wetting regime becomes heterogeneous. In this regime every pentyl group added to the surface unit cell increases the surface fraction f_1 by the same amount. When there are eight groups within the unit cell (surface 8) the fraction becomes approximately equal to one. For all concentrations higher than 2.314 C_5H_{11}/nm^2 (surface 8) the apparent contact angle remains at 180° and the wetting regime again becomes homogenous, but now on the alkylated surface. It should be noted that the range of surface pentyl concentrations of the heterogeneous wetting regime coincides with the range of surface pentyl concentrations of above mentioned wettability zones 2 and 3.

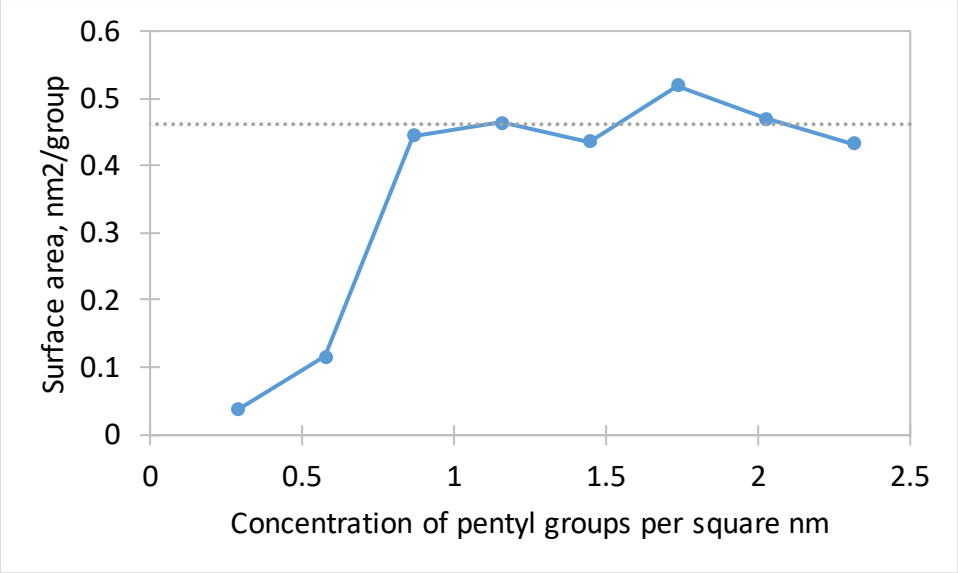

Figure 19. Surface are per one C_5H_{11} group as a function of its surface concentration. Dotted line averages values at the plateau.

In atomistic simulations analysed in this study, surfaces are smooth from a macroscopic perspective, and it has been shown previously experimentally that a minor surface roughness has no significant influence on the water/CO_2 contact angle of silica systems [32].

Conclusions

A systematic computational study of wettability of fully hydroxylated and alkylated (001) α-quartz surface under 10 MPa pressure of carbon dioxide at 300 K with respect to surface concentration of pentyl groups is performed. Considered concentrations of the alkyl groups vary from 0.29 to 4.63 C_5H_{11}/nm^2. It is shown that when the surface density of pentyl groups is increased from 0.29 to 3.18 C_5H_{11}/nm^2 the contact angle of a water droplet changes from 10-20 to 180°.

A complete description of wettability of alkylated quartz surface requires three parameters: the theoretical contact angle, the apparent contact angle and the hidden contact angle. These contact angles are determined at the tip level of pentyl groups and the level of the quartz surface. The hidden contact angle is calculated as the angle of a water "skirt", which is formed between the level of the quartz surface and the tip level of pentyl groups. The hidden contact angle remains relatively small (less than 90°) up to the threshold pentyl density of 2.604 C_5H_{11}/nm^2, after which it rather abruptly increases to 180°. We call such a behaviour the binary wettability, when the surface is either hydrophilic or extremely hydrophobic, with intermediate wetting regime observed only in a very narrow range of the surface pentyl density of 0.29 C_5H_{11}/nm^2. We conclude that this binary wettability of alkylated quartz surface originates from the steric effects preventing water molecules from reaching the quartz surface.

The theoretical and the apparent contact angles are determined as the contact angles of the spherical droplet at the level of the quartz surface and at the tip level of pentyl groups, respectively. The apparent contact angle is the angle which is most likely to be measured in an experiment and it will deviate more from the theoretical one with longer chains of chemisorpt hydrocarbons. On basis of the theoretical and the apparent contact angles four wettability zones can be identified. In the zone 1 (water wet zone) the pentyl density is in range 0.289-0.579 C_5H_{11}/nm^2, and the contact angle is in range 15-40°. In the zone 2 (intermediate wet zone) the pentyl density is in range 0.868-1.447 C_5H_{11}/nm^2, and the contact angle is in range 77-122°. In the zone 3 (CO_2 wet zone) the pentyl

density is in range 1.736-2.314 C_5H_{11}/nm^2, and the contact angle is in range 143-180°. In the zone 4 (extremely hydrophobic zone) the pentyl density is 2.604 C_5H_{11}/nm^2 or higher, and the contact angle is 180°. Additionally, the wettability regime in zones 2 and 3 can be regarded as heterogeneous.

A possible future research direction is the modification of the quartz surface with varied alkyl chain length. It is reasonable to expect that in this case the contact angle will be mostly determined by the parameters for the hydrocarbons, thus making the surface even more hydrophobic.

Supporting Information

Surface hydroxyl group concentration vs surface pentyl group concentration, water iso-density charts for surfaces 1 through 11, simulation snapshots for surfaces 1 through 11, simulation snapshots with removed pentyl groups for surfaces 1 through 11.

Acknowledgments

This work was supported by resources provided by the Pawsey Supercomputing Centre with funding from the Australian Government and the Government of Western Australia.

References

1. Iglauer, S.; Al-Yaseri, A. Z.; Rezaee, R.; Lebedev, M., CO2 wettability of caprocks: Implications for structural storage capacity and containment security. *Geophysical Research Letters* **2015,** *42* (21), 9279-9284.
2. Iglauer, S., CO2–Water–Rock Wettability: Variability, Influencing Factors, and Implications for CO2 Geostorage. *Accounts of Chemical Research* **2017,** *50* (5), 1134-1142.
3. Ali, M.; Al-Anssari, S.; Arif, M.; Barifcani, A.; Sarmadivaleh, M.; Stalker, L.; Lebedev, M.; Iglauer, S., Organic acid concentration thresholds for ageing of carbonate minerals: Implications for CO2 trapping/storage. *Journal of Colloid and Interface Science* **2019,** *534*, 88-94.
4. Balascio, J. F.; Lind, T., The growth of piezoelectric alpha quartz crystals. *Current Opinion in Solid State and Materials Science* **1997,** *2* (5), 588-592.
5. Nash, T.; Allison, A. C.; Harington, J. S., Physico-Chemical Properties of Silica in Relation to its Toxicity. *Nature* **1966,** *210*, 259.
6. Mautner, M. N.; Abdelsayed, V.; El-Shall, M. S.; Thrower, J. D.; Green, S. D.; Collings, M. P.; McCoustra, M. R. S., Meteorite nanoparticles as models for interstellar grains: Synthesis and preliminary characterisation. *Faraday Discussions* **2006,** *133* (0), 103-112.
7. Wang, D.-M.; Xu, Y.-M.; He, D.-M.; Guan, J.; Zhang, O.-M., Investigation of mineral composition of oil shale. *Asia-Pacific Journal of Chemical Engineering* **2009,** *4* (5), 691-697.
8. Demuth, T.; Jeanvoine, Y.; Hafner, J.; Ángyán, J. G., Polymorphism in silica studied in the local density and generalized-gradient approximations. *Journal of Physics: Condensed Matter* **1999,** *11* (19), 3833.
9. Swamy, V.; Saxena, S. K.; Sundman, B.; Zhang, J., A thermodynamic assessment of silica phase diagram. *Journal of Geophysical Research: Solid Earth* **1994,** *99* (B6), 11787-11794.
10. de Leeuw, N. H.; Higgins, F. M.; Parker, S. C., Modeling the Surface Structure and Stability of α-Quartz. *The Journal of Physical Chemistry B* **1999,** *103* (8), 1270-1277.
11. Murashov, V. V., Reconstruction of Pristine and Hydrolyzed Quartz Surfaces. *The Journal of Physical Chemistry B* **2005,** *109* (9), 4144-4151.
12. Yang, J.; Wang, E. G., Water adsorption on hydroxylated alpha-quartz (0001) surfaces: From monomer to flat bilayer. *Physical Review B* **2006,** *73* (3), 035406.
13. Goumans, T. P. M.; Wander, A.; Brown, W. A.; Catlow, C. R. A., Structure and stability of the (001) α-quartz surface. *Physical Chemistry Chemical Physics* **2007,** *9* (17), 2146-2152.
14. Malyi, O. I.; Kulish, V. V.; Persson, C., In search of new reconstructions of (001) α-quartz surface: a first principles study. *RSC Advances* **2014,** *4* (98), 55599-55603.

15. Chen, Y.-W.; Cao, C.; Cheng, H.-P., Finding stable α-quartz (0001) surface structures via simulations. *Applied Physics Letters* **2008,** *93* (18), 181911.
16. Eder, S. D.; Fladischer, K.; Yeandel, S. R.; Lelarge, A.; Parker, S. C.; Søndergård, E.; Holst, B., A Giant Reconstruction of α-quartz (0001) Interpreted as Three Domains of Nano Dauphine Twins. *Scientific Reports* **2015,** *5*, 14545.
17. Feya, O. D.; Wang, Q.; Lepeshkin, S. V.; Baturin, V. S.; Uspenskii, Y. A.; Oganov, A. R., Tetrahedral honeycomb surface reconstructions of quartz, cristobalite and stishovite. *Scientific Reports* **2018,** *8* (1), 11947.
18. Emami, F. S.; Puddu, V.; Berry, R. J.; Varshney, V.; Patwardhan, S. V.; Perry, C. C.; Heinz, H., Force Field and a Surface Model Database for Silica to Simulate Interfacial Properties in Atomic Resolution. *Chemistry of Materials* **2014,** *26* (8), 2647-2658.
19. Zhuravlev, L. T., The surface chemistry of amorphous silica. Zhuravlev model. *Colloids and Surfaces A: Physicochemical and Engineering Aspects* **2000,** *173* (1), 1-38.
20. Iler, R. K., *The Chemistry of Silica: Solubility, Polymerization, Colloid and Surface Properties and Biochemistry of Silica*. John Wiley & Sons (Wiley-Interscience Publication): 1979; p 896.
21. Iglauer, S.; Pentland, C. H.; Busch, A., CO2 wettability of seal and reservoir rocks and the implications for carbon geo-sequestration. *Water Resources Research* **2014,** *51* (1), 729-774.
22. Anderson, R. S.; Anderson, S. P., *Geomorphology: The Mechanics and Chemistry of Landscapes*. Cambridge University Press: 2010.
23. Marshall, C. P.; Fairbridge, R. W., *Encyclopedia of Geochemistry*. Springer: 1999.
24. IPCC *Carbon Dioxide Capture and Storage*; Intergovernmental Panel on Climate Change: 2005, 2005.
25. Mazurek, A.; Pogorzelski, S. J.; Boniewicz-Szmyt, K., Adsorption of natural surfactants present in sea waters at surfaces of minerals: contact angle measurements. **2009,** *v. 51*.
26. Lamb, R. N.; Furlong, D. N., Controlled wettability of quartz surfaces. *Journal of the Chemical Society, Faraday Transactions 1: Physical Chemistry in Condensed Phases* **1982,** *78* (1), 61-73.
27. Roshan, H.; Al-Yaseri, A. Z.; Sarmadivaleh, M.; Iglauer, S., On wettability of shale rocks. *Journal of Colloid and Interface Science* **2016,** *475*, 104-111.
28. Broseta, D.; Tonnet, N.; Shah, V., Are rocks still water-wet in the presence of dense CO2 or H2S? *Geofluids* **2012,** *12* (4), 280-294.
29. Espinoza, D. N.; Santamarina, J. C., Water-CO2-mineral systems: Interfacial tension, contact angle, and diffusion—Implications to CO2 geological storage. *Water Resources Research* **2010,** *46* (7).
30. Sklodowska, A.; Matlakowska, R., Influence of exopolymers produced by bacterial cells on hydrophobicity of substrate surface. *Biotechnology Techniques* **1997,** *11* (11), 837-840.
31. Al-Yaseri, A. Z.; Roshan, H.; Lebedev, M.; Barifcani, A.; Iglauer, S., Dependence of quartz wettability on fluid density. *Geophysical Research Letters* **2016,** *43* (8), 3771-3776.
32. Al-Yaseri, A. Z.; Lebedev, M.; Barifcani, A.; Iglauer, S., Receding and advancing (CO2+brine+quartz) contact angles as a function of pressure, temperature, surface roughness, salt type and salinity. *The Journal of Chemical Thermodynamics* **2016,** *93*, 416-423.
33. Bracco, G.; Holst, B., *Surface Science Techniques*. Springer: 2013.
34. Sarmadivaleh, M.; Al-Yaseri, A. Z.; Iglauer, S., Influence of temperature and pressure on quartz–water–CO2 contact angle and CO2–water interfacial tension. *Journal of Colloid and Interface Science* **2015,** *441*, 59-64.
35. Saraji, S.; Goual, L.; Piri, M.; Plancher, H., Wettability of Supercritical Carbon Dioxide/Water/Quartz Systems: Simultaneous Measurement of Contact Angle and Interfacial Tension at Reservoir Conditions. *Langmuir* **2013,** *29* (23), 6856-6866.
36. Kaveh, N. S.; Rudolph, E. S. J.; van Hemert, P.; Rossen, W. R.; Wolf, K. H., Wettability Evaluation of a CO2/Water/Bentheimer Sandstone System: Contact Angle, Dissolution, and Bubble Size. *Energy & Fuels* **2014,** *28* (6), 4002-4020.
37. Koh, P. T. L.; Hao, F. P.; Smith, L. K.; Chau, T. T.; Bruckard, W. J., The effect of particle shape and hydrophobicity in flotation. *International Journal of Mineral Processing* **2009,** *93* (2), 128-134.

38. Deng, Y.; Xu, L.; Lu, H.; Wang, H.; Shi, Y., Direct measurement of the contact angle of water droplet on quartz in a reservoir rock with atomic force microscopy. *Chemical Engineering Science* **2018,** *177*, 445-454.
39. Giovambattista, N.; Debenedetti, P. G.; Rossky, P. J., Effect of Surface Polarity on Water Contact Angle and Interfacial Hydration Structure. *The Journal of Physical Chemistry B* **2007,** *111* (32), 9581-9587.
40. Bagherzadeh, S. A.; Englezos, P.; Alavi, S.; Ripmeester, J. A., Influence of Hydrated Silica Surfaces on Interfacial Water in the Presence of Clathrate Hydrate Forming Gases. *The Journal of Physical Chemistry C* **2012,** *116* (47), 24907-24915.
41. Iglauer, S.; Mathew, M. S.; Bresme, F., Molecular dynamics computations of brine–CO2 interfacial tensions and brine–CO2–quartz contact angles and their effects on structural and residual trapping mechanisms in carbon geo-sequestration. *Journal of Colloid and Interface Science* **2012,** *386* (1), 405-414.
42. McCaughan, J.; Iglauer, S.; Bresme, F., Molecular Dynamics Simulation of Water/CO2-quartz Interfacial Properties: Application to Subsurface Gas Injection. *Energy Procedia* **2013,** *37*, 5387-5402.
43. Chen, C.; Wan, J.; Li, W.; Song, Y., Water contact angles on quartz surfaces under supercritical CO2 sequestration conditions: Experimental and molecular dynamics simulation studies. *International Journal of Greenhouse Gas Control* **2015,** *42*, 655-665.
44. Liu, S.; Yang, X.; Qin, Y., Molecular dynamics simulation of wetting behavior at CO2/water/solid interfaces. *Chinese Science Bulletin* **2010,** *55* (21), 2252-2257.
45. Chen, C.; Zhang, N.; Li, W.; Song, Y., Water Contact Angle Dependence with Hydroxyl Functional Groups on Silica Surfaces under CO2 Sequestration Conditions. *Environmental Science & Technology* **2015,** *49* (24), 14680-14687.
46. Chen, C.; Chai, Z.; Shen, W.; Li, W.; Song, Y., Wettability of Supercritical CO2–Brine–Mineral: The Effects of Ion Type and Salinity. *Energy & Fuels* **2017,** *31* (7), 7317-7324.
47. Chen, C.; Chai, Z.; Shen, W.; Li, W., Effects of Impurities on CO2 Sequestration in Saline Aquifers: Perspective of Interfacial Tension and Wettability. *Industrial & Engineering Chemistry Research* **2018,** *57* (1), 371-379.
48. Tenney, C. M.; Cygan, R. T., Molecular Simulation of Carbon Dioxide, Brine, and Clay Mineral Interactions and Determination of Contact Angles. *Environmental Science & Technology* **2014,** *48* (3), 2035-2042.
49. Tsuji, S.; Liang, Y.; Kunieda, M.; Takahashi, S.; Matsuoka, T., Molecular Dynamics Simulations of the CO2-Water-silica Interfacial Systems. *Energy Procedia* **2013,** *37*, 5435-5442.
50. Liang, Y.; Tsuji, S.; Jia, J.; Tsuji, T.; Matsuoka, T., Modeling CO2–Water–Mineral Wettability and Mineralization for Carbon Geosequestration. *Accounts of Chemical Research* **2017,** *50* (7), 1530-1540.
51. Javanbakht, G.; Sedghi, M.; Welch, W.; Goual, L., Molecular Dynamics Simulations of CO2/Water/Quartz Interfacial Properties: Impact of CO2 Dissolution in Water. *Langmuir* **2015,** *31* (21), 5812-5819.
52. Buckley, J. S.; Bousseau, C.; Liu, Y., Wetting Alteration by Brine and Crude Oil: From Contact Angles to Cores. *SPE-30765-PA* **1996,** *1* (03), 341-350.
53. Arif, M.; Barifcani, A.; Lebedev, M.; Iglauer, S., Structural trapping capacity of oil-wet caprock as a function of pressure, temperature and salinity. *International Journal of Greenhouse Gas Control* **2016,** *50*, 112-120.
54. Todorov, I. T.; Smith, W.; Trachenko, K.; Dove, M. T., DL_POLY_3: new dimensions in molecular dynamics simulations via massive parallelism. *Journal of Materials Chemistry* **2006,** *16* (20), 1911-1918.
55. Bush, I. J.; Todorov, I. T.; Smith, W., A DAFT DL_POLY distributed memory adaptation of the Smoothed Particle Mesh Ewald method. *Computer Physics Communications* **2006,** *175* (5), 323-329.
56. Giannozzi, P.; Baroni, S.; Bonini, N.; Calandra, M.; Car, R.; Cavazzoni, C.; Ceresoli, D.; Chiarotti Guido, L.; Cococcioni, M.; Dabo, I.; al, e., QUANTUM ESPRESSO: a modular and open-source software

project for quantum simulations of materials. *Journal of Physics: Condensed Matter* **2009,** *21* (39), 395502.
57. Giannozzi, P.; Andreussi, O.; Brumme, T.; Bunau, O.; Nardelli, M. B.; Calandra, M.; Car, R.; Cavazzoni, C.; Ceresoli, D.; Cococcioni, M.; al, e., Advanced capabilities for materials modelling with Q uantum ESPRESSO. *Journal of Physics: Condensed Matter* **2017,** *29* (46), 465901.
58. Bader, R. F. W., *Atoms in Molecules: A Quantum Theory*. Oxford University Press: 1994; p 456.
59. Henkelman, G.; Arnaldsson, A.; Jónsson, H., A fast and robust algorithm for Bader decomposition of charge density. *Computational Materials Science* **2006,** *36* (3), 354-360.
60. Sanville, E.; Kenny, S. D.; Smith, R.; Henkelman, G., Improved grid-based algorithm for Bader charge allocation. *Journal of Computational Chemistry* **2007,** *28* (5), 899-908.
61. Tang, W.; Sanville, E.; Henkelman, G., A grid-based Bader analysis algorithm without lattice bias. *Journal of Physics: Condensed Matter* **2009,** *21* (8), 084204.
62. Yu, M.; Trinkle, D. R., Accurate and efficient algorithm for Bader charge integration. *The Journal of Chemical Physics* **2011,** *134* (6), 064111.
63. Humphrey, W.; Dalke, A.; Schulten, K., VMD: Visual molecular dynamics. *Journal of Molecular Graphics* **1996,** *14* (1), 33-38.
64. Momma, K.; Izumi, F., VESTA: a three-dimensional visualization system for electronic and structural analysis. *Journal of Applied Crystallography* **2008,** *41* (3), 653-658.
65. Swope, W. C.; Andersen, H. C.; Berens, P. H.; Wilson, K. R., A computer simulation method for the calculation of equilibrium constants for the formation of physical clusters of molecules: Application to small water clusters. *The Journal of Chemical Physics* **1982,** *76* (1), 637-649.
66. Hoover, W. G., Canonical dynamics: Equilibrium phase-space distributions. *Physical Review A* **1985,** *31* (3), 1695-1697.
67. Nosé, S., A molecular dynamics method for simulations in the canonical ensemble. *Molecular Physics* **1984,** *52* (2), 255-268.
68. Essmann, U.; Perera, L.; Berkowitz, M. L.; Darden, T.; Lee, H.; Pedersen, L. G., A smooth particle mesh Ewald method. *The Journal of Chemical Physics* **1995,** *103* (19), 8577-8593.
69. Darden, T.; York, D.; Pedersen, L., Particle mesh Ewald: An N·log(N) method for Ewald sums in large systems. *The Journal of Chemical Physics* **1993,** *98* (12), 10089-10092.
70. Berendsen, H. J. C.; Postma, J. P. M.; van Gunsteren, W. F.; Hermans, J., Interaction Models for Water in Relation to Protein Hydration. In *Intermolecular Forces: Proceedings of the Fourteenth Jerusalem Symposium on Quantum Chemistry and Biochemistry Held in Jerusalem, Israel, April 13–16, 1981*, Pullman, B., Ed. Springer Netherlands: Dordrecht, 1981; pp 331-342.
71. Cygan, R. T.; Liang, J.-J.; Kalinichev, A. G., Molecular Models of Hydroxide, Oxyhydroxide, and Clay Phases and the Development of a General Force Field. *The Journal of Physical Chemistry B* **2004,** *108* (4), 1255-1266.
72. Harris, J. G.; Yung, K. H., Carbon Dioxide's Liquid-Vapor Coexistence Curve And Critical Properties as Predicted by a Simple Molecular Model. *The Journal of Physical Chemistry* **1995,** *99* (31), 12021-12024.
73. Mayo, S. L.; Olafson, B. D.; Goddard, W. A., DREIDING: a generic force field for molecular simulations. *The Journal of Physical Chemistry* **1990,** *94* (26), 8897-8909.
74. Todorov, I. T.; Smith, W. *The DL_POLY_4 user manual. Version 4.08*; STFC Daresbury Laboratory: 2016.
75. Lorentz, H. A., Ueber die Anwendung des Satzes vom Virial in der kinetischen Theorie der Gase. *Annalen der Physik* **1881,** *248* (1), 127-136.
76. Berthelot, D., Sur le mélange des gaz. *Comptes rendus hebdomadaires des séances de l'Académie des Sciences* **1898,** *126*, 1703-1855.
77. Adeagbo, W. A.; Doltsinis, N. L.; Klevakina, K.; Renner, J., Transport Processes at α-Quartz–Water Interfaces: Insights from First-Principles Molecular Dynamics Simulations. *ChemPhysChem* **2008,** *9* (7), 994-1002.

78. Monkhorst, H. J.; Pack, J. D., Special points for Brillouin-zone integrations. *Physical Review B* **1976,** *13* (12), 5188-5192.
79. Blöchl, P. E., Projector augmented-wave method. *Physical Review B* **1994,** *50* (24), 17953-17979.
80. www.quantum-espresso.org Quantum ESPRESSO. www.quantum-espresso.org.
81. Perdew, J. P.; Burke, K.; Ernzerhof, M., Generalized Gradient Approximation Made Simple. *Physical Review Letters* **1996,** *77* (18), 3865-3868.
82. Levien, L.; Prewitt, C. T.; Weidner, D. J., Structure and elastic properties of quartz at pressure. *American Mineralogist* **1980,** *65* (9-10), 920-930.
83. webbook.nist.gov NIST Chemistry WebBook. https://webbook.nist.gov/chemistry/.
84. Broyden, C. G., The Convergence of a Class of Double-rank Minimization Algorithms 1. General Considerations. *IMA Journal of Applied Mathematics* **1970,** *6* (1), 76-90.
85. Fletcher, R., A new approach to variable metric algorithms. *The Computer Journal* **1970,** *13* (3), 317-322.
86. Goldfarb, D., A Family of Variable-Metric Methods Derived by Variational Means. *Mathematics of Computation* **1970,** *24* (109), 23-26.
87. Shanno, D. F., Conditioning of Quasi-Newton Methods for Function Minimization. *Mathematics of Computation* **1970,** *24* (111), 647-656.
88. Cassie, A. B. D.; Baxter, S., Wettability of porous surfaces. *Transactions of the Faraday Society* **1944,** *40* (0), 546-551.

TOC Graphic

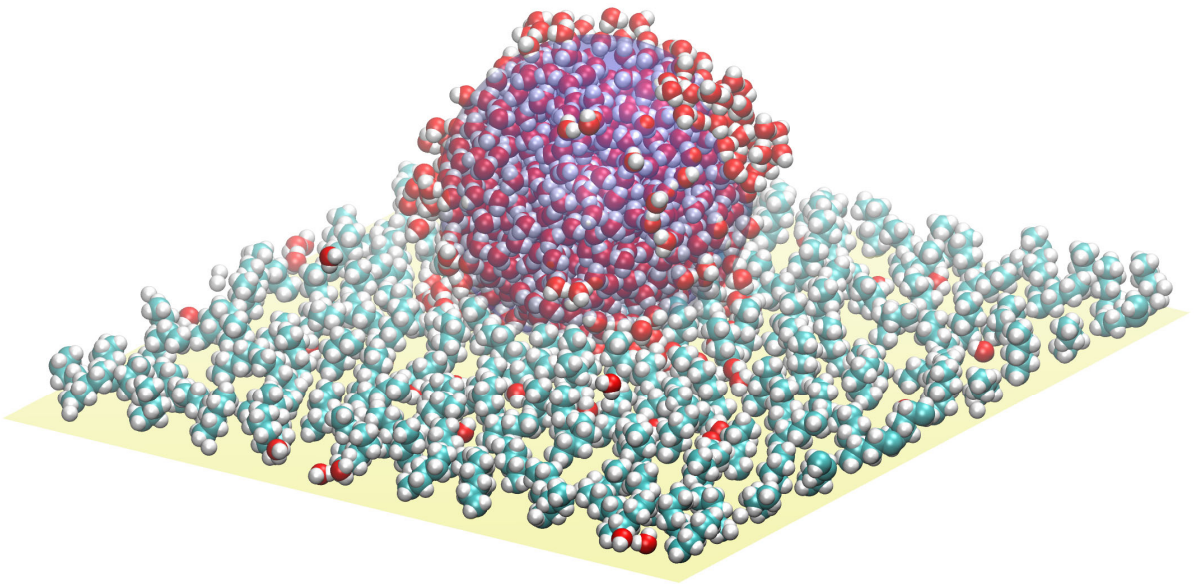

Wettability of Fully Hydroxylated and Alkylated (001) alpha-Quartz Surface in Carbon Dioxide Atmosphere

Aleksandr Abramov*, Stefan Iglauer, Alireza Keshavarz, School of Engineering, Edith Cowan University, 270 Joondalup Drive, Joondalup, WA 6027, Western Australia, Australia

*aabramov@our.ecu.edu.au

Surface Hydroxyl Group Concentration vs Surface Pentyl Group Concentration

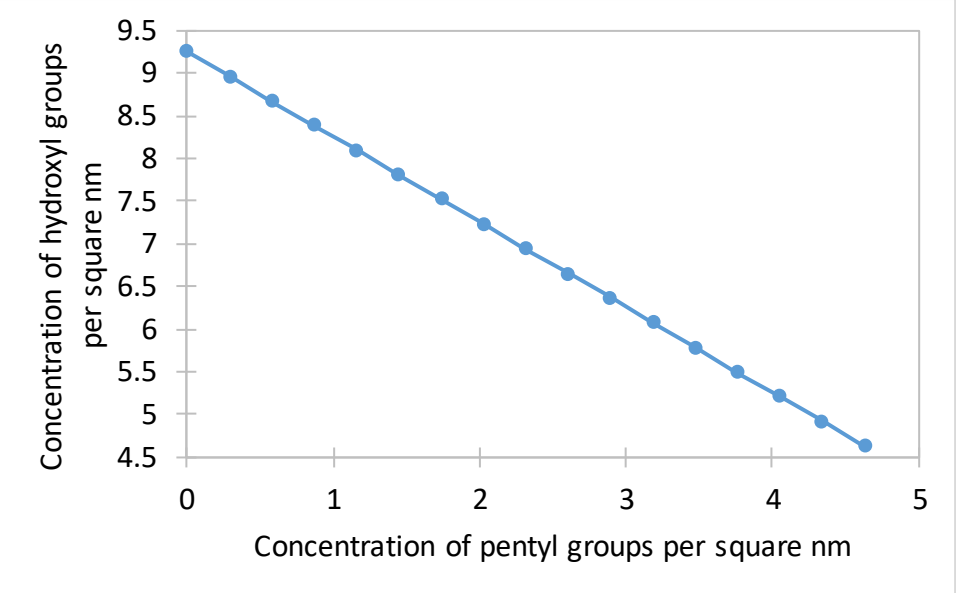

Figure S1. Surface hydroxyl group concentration as a function of surface pentyl group concentration.

Water Iso-Density Charts for Surfaces 1 Through 11

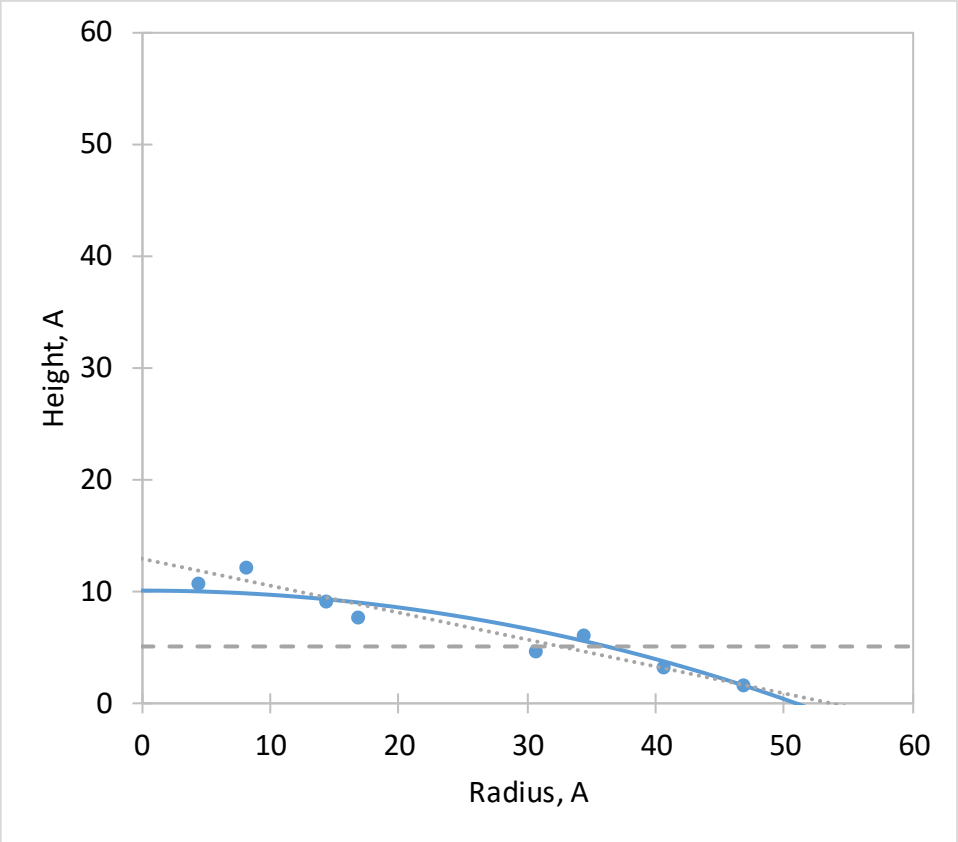

Figure S2. Water iso-density chart for quartz surface (surface 1) with concentration of pentyl groups 0.289 C_5H_{11} per square nm. The iso-density data points are shown with blue dots, fitted circle is shown with blue line, the tip level of the pentyl groups is shown with the dashed line, the dotted line illustrates the planar projection of the water "skirt".

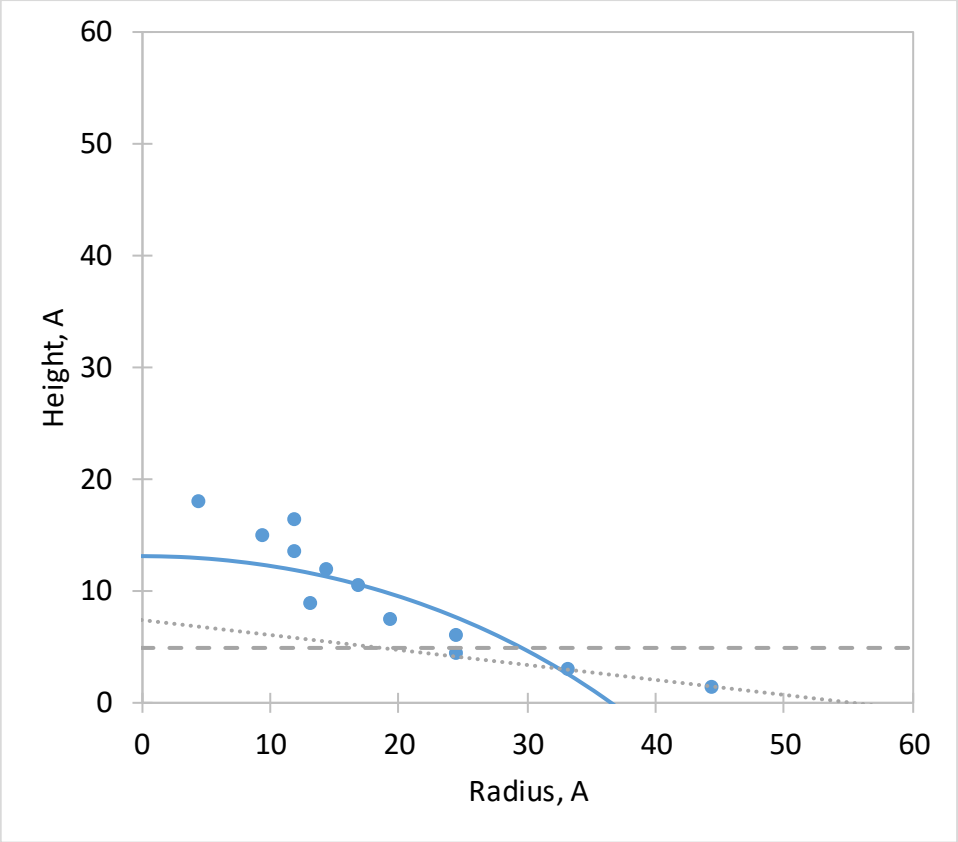

Figure S3. Water iso-density chart for quartz surface (surface 2) with concentration of pentyl groups 0.579 C_5H_{11} per square nm. The iso-density data points are shown with blue dots, fitted circle is shown with blue line, the tip level of the pentyl groups is shown with the dashed line, the dotted line illustrates the planar projection of the water "skirt".

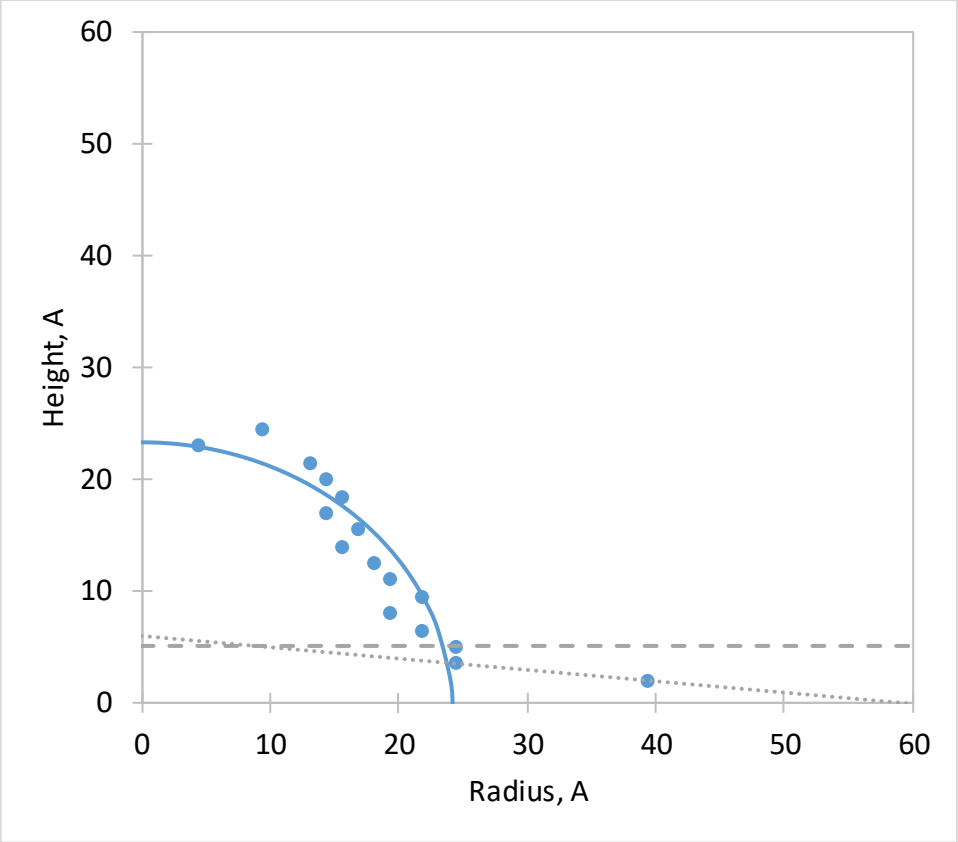

Figure S4. Water iso-density chart for quartz surface (surface 3) with concentration of pentyl groups 0.868 C_5H_{11} per square nm. The iso-density data points are shown with blue dots, fitted circle is shown with blue line, the tip level of the pentyl groups is shown with the dashed line, the dotted line illustrates the planar projection of the water "skirt".

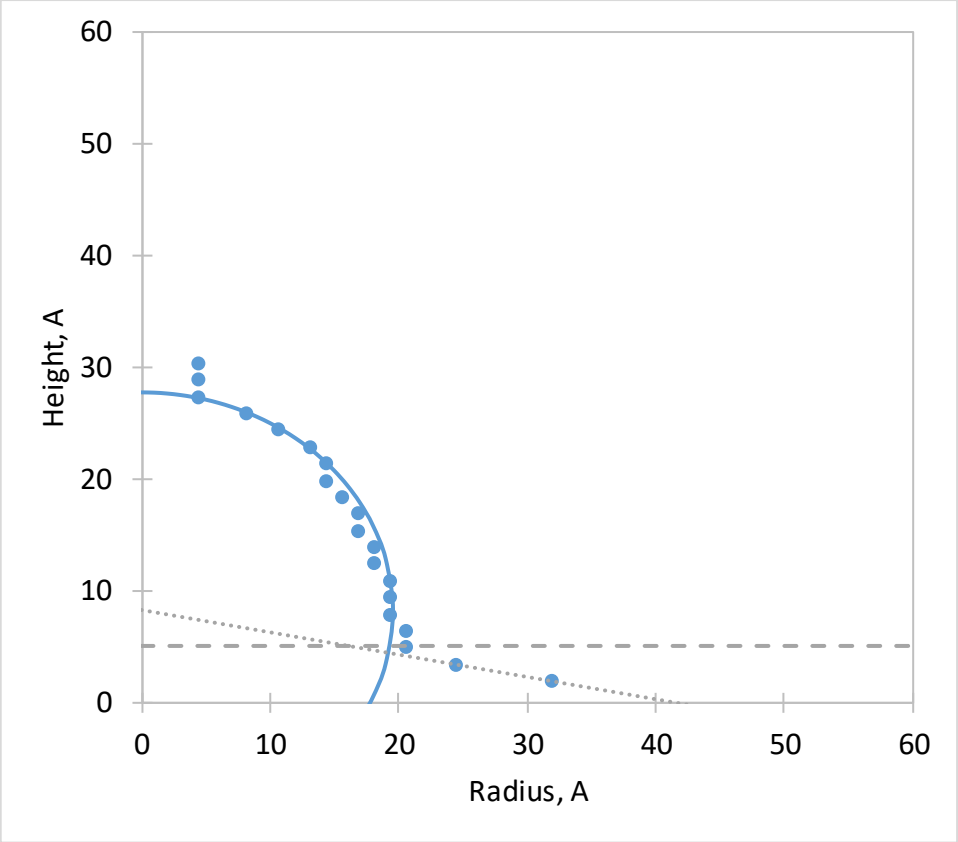

Figure S5. Water iso-density chart for quartz surface (surface 4) with concentration of pentyl groups 1.157 C_5H_{11} per square nm. The iso-density data points are shown with blue dots, fitted circle is shown with blue line, the tip level of the pentyl groups is shown with the dashed line, the dotted line illustrates the planar projection of the water "skirt".

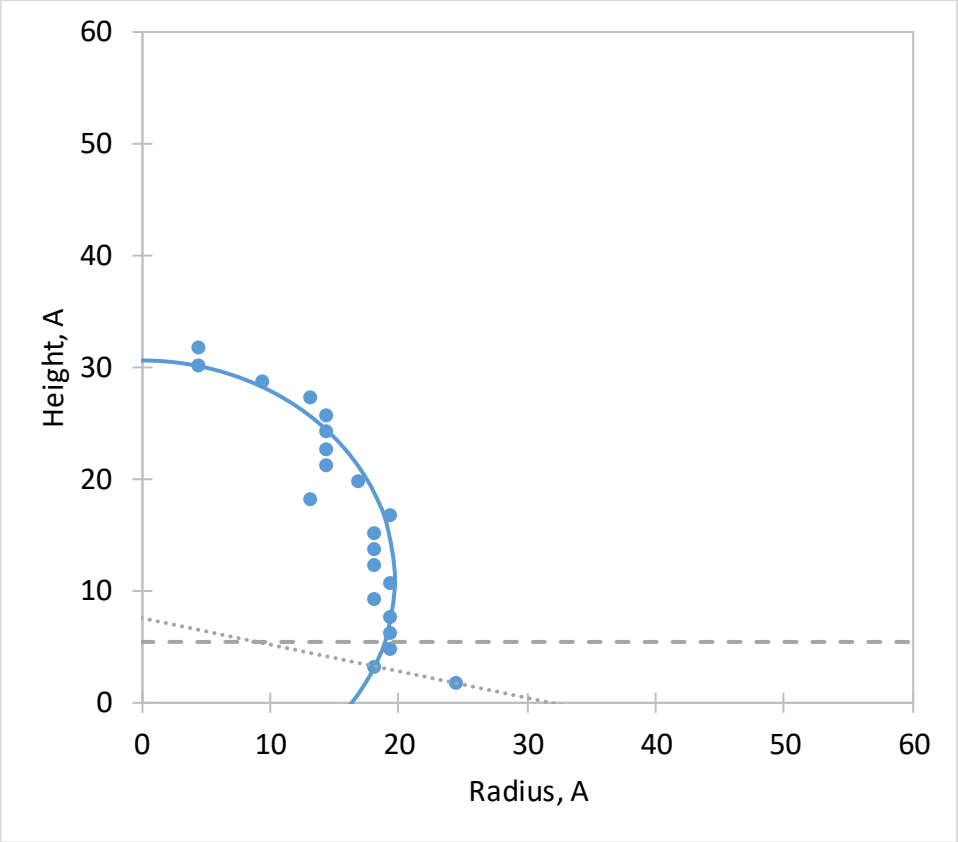

Figure S6. Water iso-density chart for quartz surface (surface 5) with concentration of pentyl groups 1.447 C_5H_{11} per square nm. The iso-density data points are shown with blue dots, fitted circle is shown with blue line, the tip level of the pentyl groups is shown with the dashed line, the dotted line illustrates the planar projection of the water "skirt".

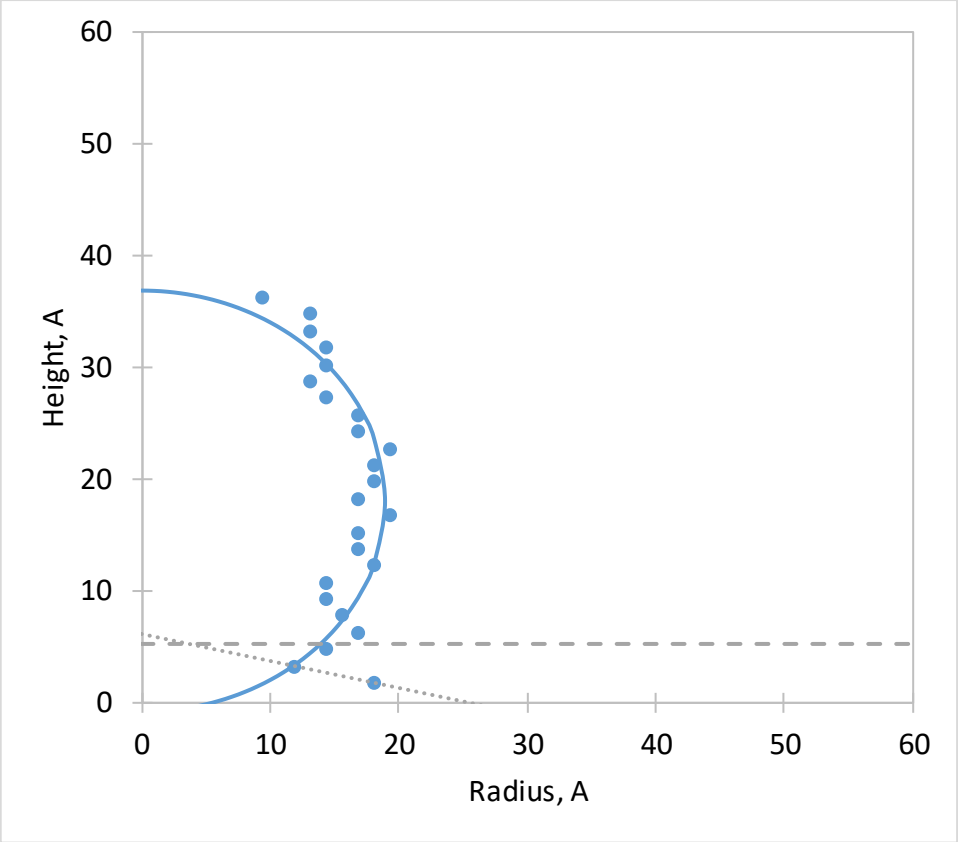

Figure S7. Water iso-density chart for quartz surface (surface 6) with concentration of pentyl groups 1.736 C_5H_{11} per square nm. The iso-density data points are shown with blue dots, fitted circle is shown with blue line, the tip level of the pentyl groups is shown with the dashed line, the dotted line illustrates the planar projection of the water "skirt".

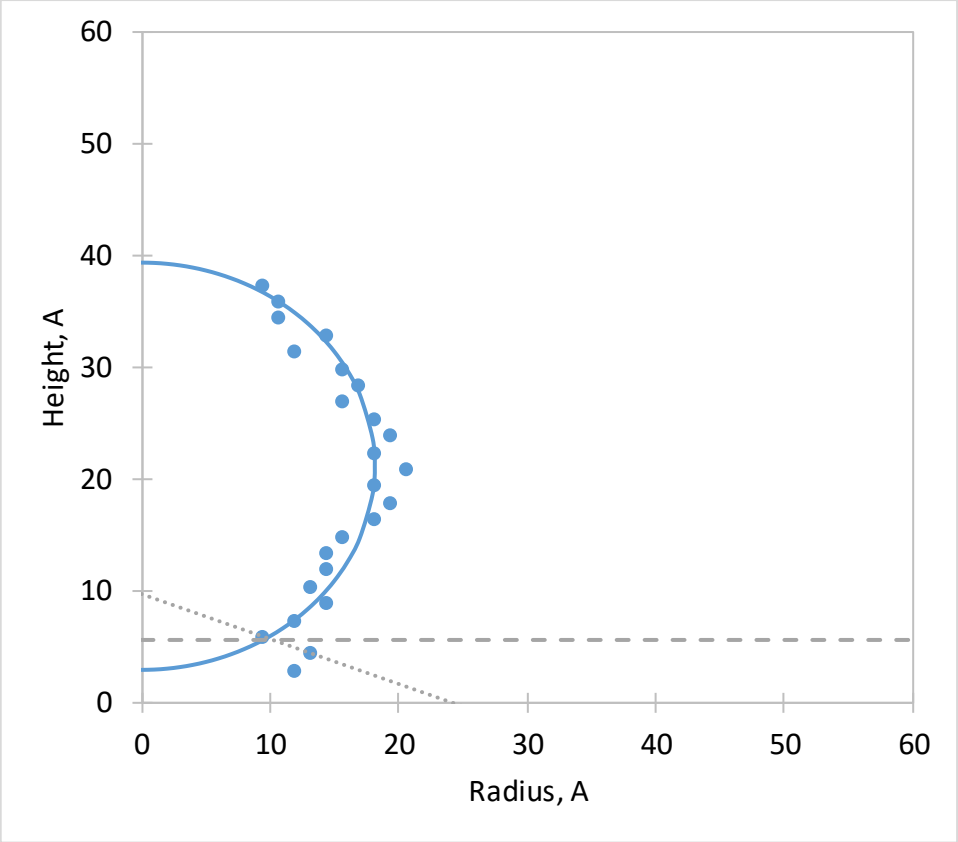

Figure S8. Water iso-density chart for quartz surface (surface 7) with concentration of pentyl groups 2.025 C_5H_{11} per square nm. The iso-density data points are shown with blue dots, fitted circle is shown with blue line, the tip level of the pentyl groups is shown with the dashed line, the dotted line illustrates the planar projection of the water "skirt".

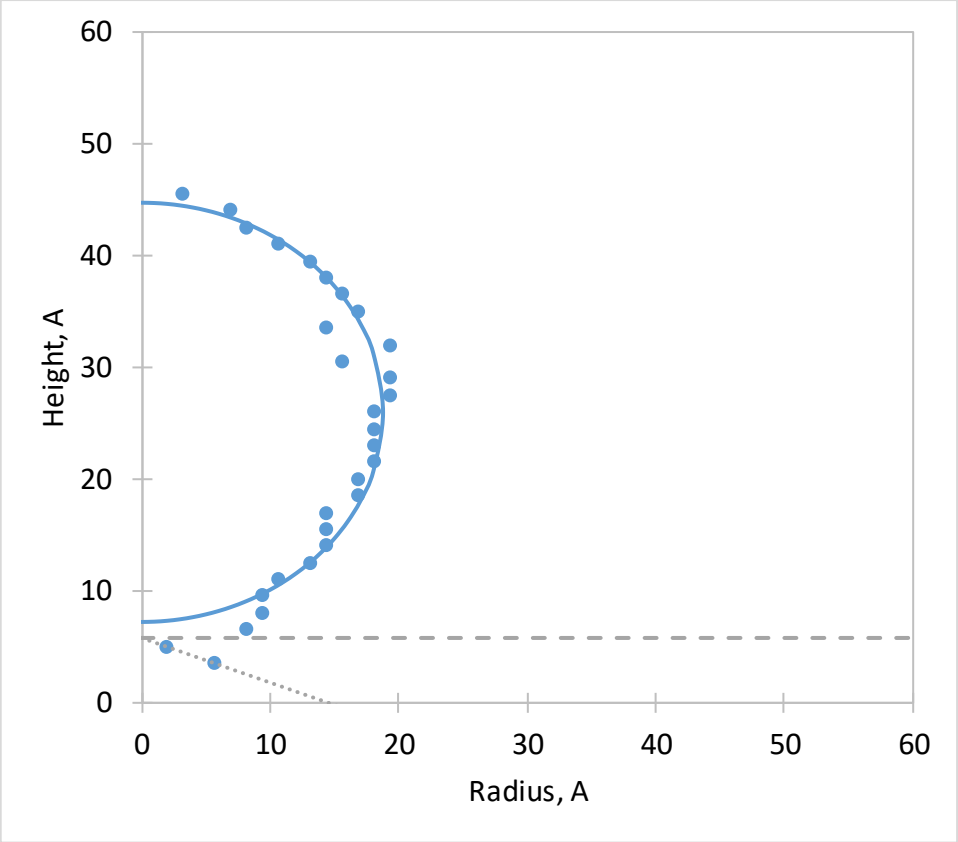

Figure S9. Water iso-density chart for quartz surface (surface 8) with concentration of pentyl groups 2.314 C_5H_{11} per square nm. The iso-density data points are shown with blue dots, fitted circle is shown with blue line, the tip level of the pentyl groups is shown with the dashed line, the dotted line illustrates the planar projection of the water "skirt".

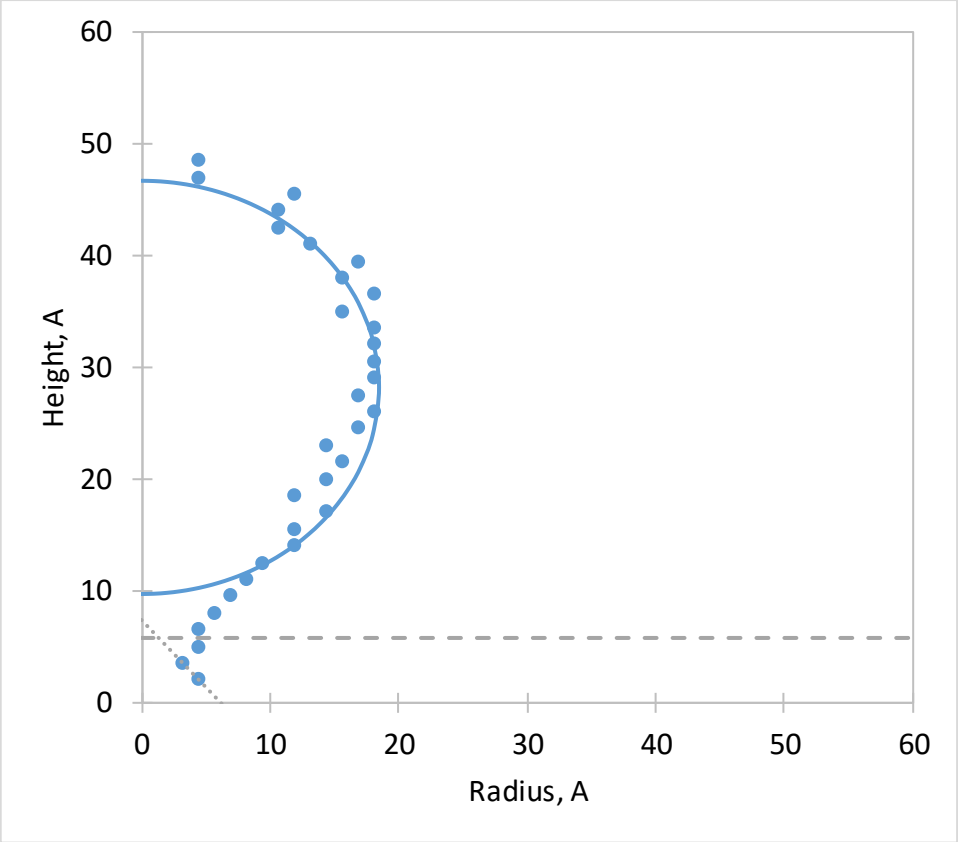

Figure S10. Water iso-density chart for quartz surface (surface 9) with concentration of pentyl groups 2.604 C_5H_{11} per square nm. The iso-density data points are shown with blue dots, fitted circle is shown with blue line, the tip level of the pentyl groups is shown with the dashed line, the dotted line illustrates the planar projection of the water "skirt".

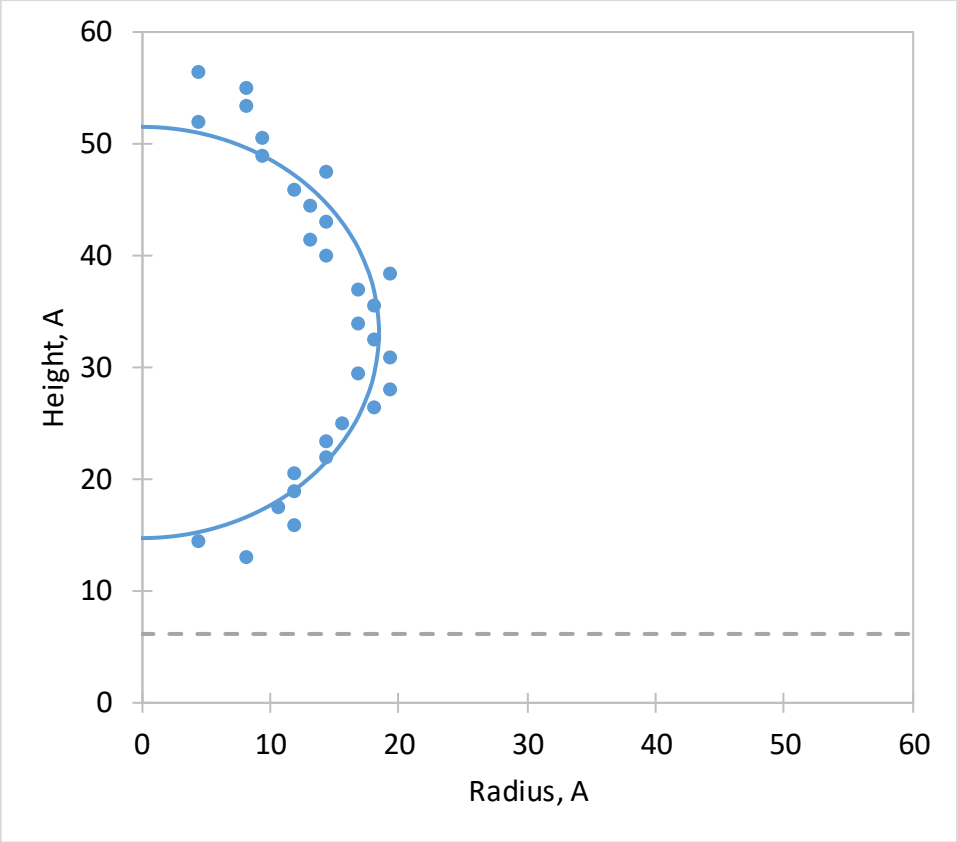

Figure S11. Water iso-density chart for quartz surface (surface 10) with concentration of pentyl groups 2.893 C_5H_{11} per square nm. The iso-density data points are shown with blue dots, fitted circle is shown with blue line, the tip level of the pentyl groups is shown with the dashed line.

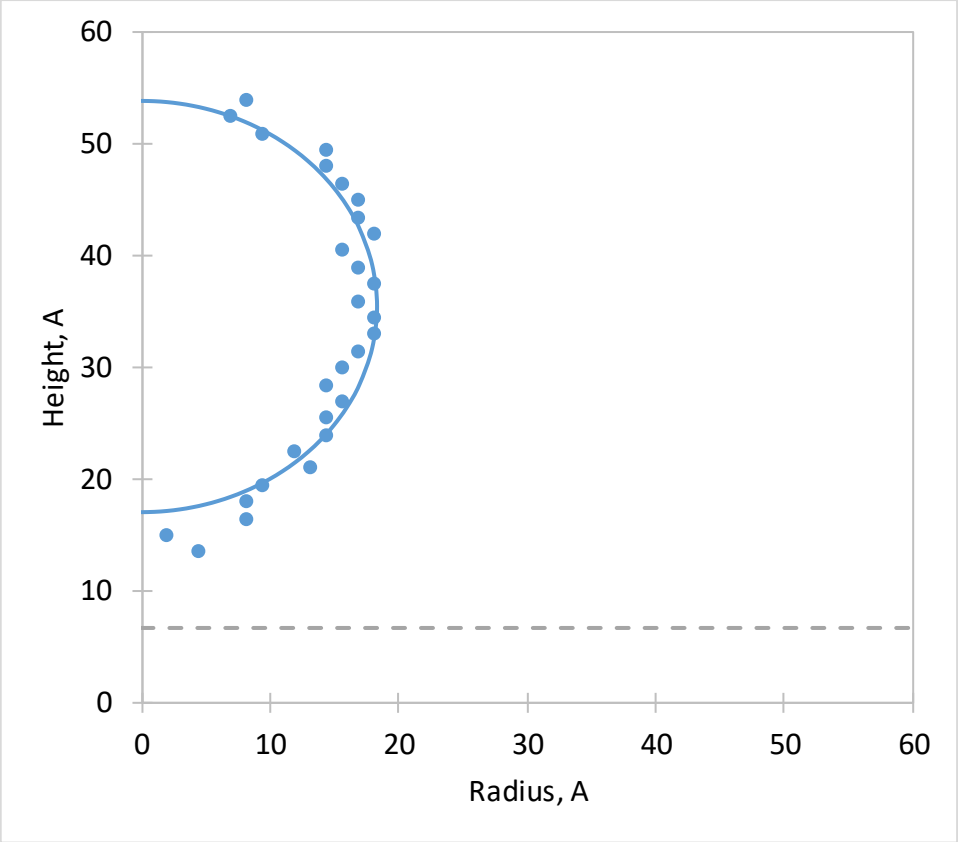

Figure S12. Water iso-density chart for quartz surface (surface 11) with concentration of pentyl groups 3.182 C_5H_{11} per square nm. The iso-density data points are shown with blue dots, fitted circle is shown with blue line, the tip level of the pentyl groups is shown with the dashed line.

Simulation Snapshots for Surfaces 1 Through 11

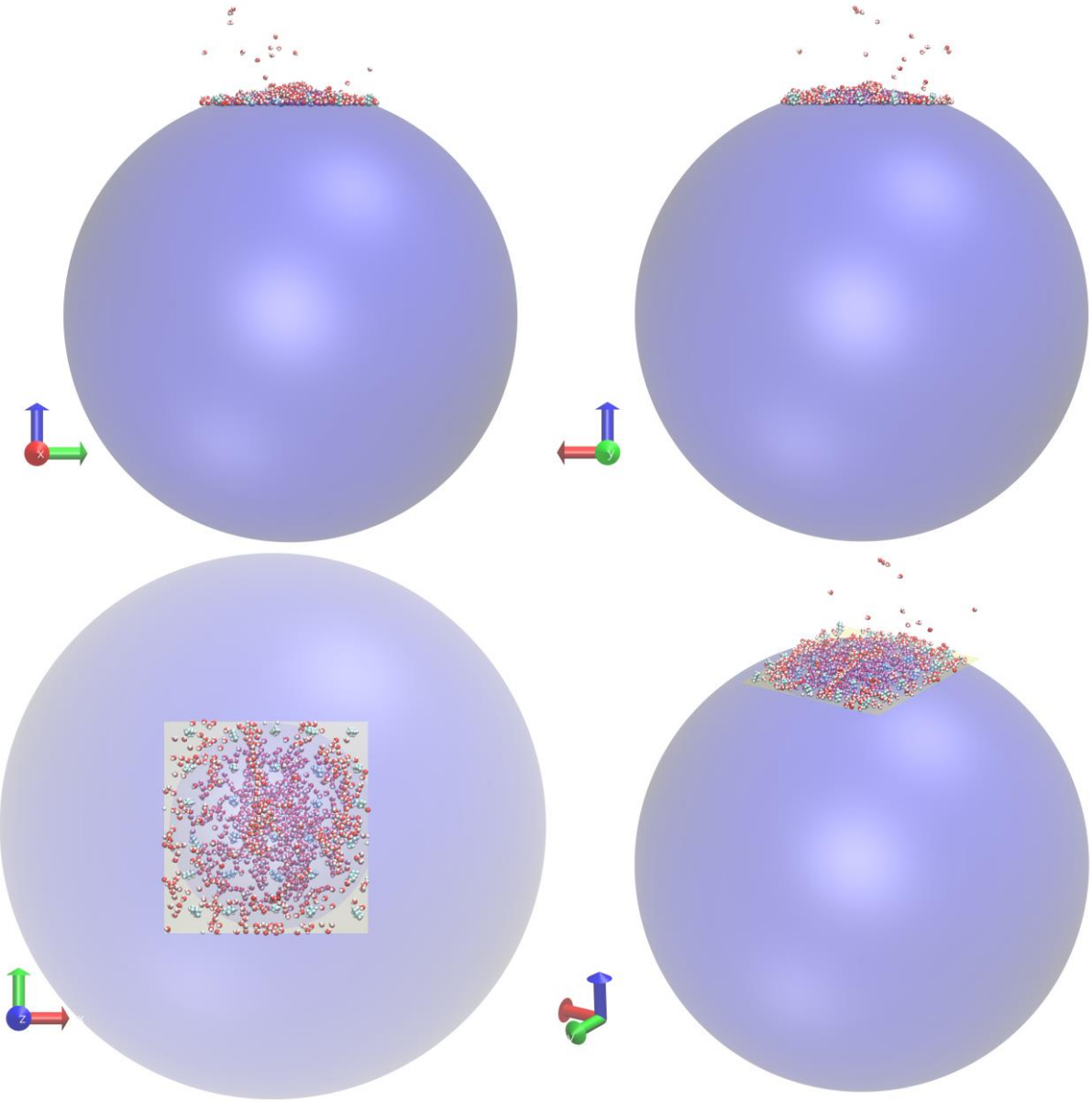

Figure S13. Simulation snapshot of the quartz surface with pentyl concentration 0.289 groups per square nm (surface 1). View along x axis: top left; view along y axis: top right; view along z axis: bottom left; isometric view: bottom right. The sphere fitted to the iso-density chart is illustrated in light purple color. The surface is illustrated with square in light yellow color. Water molecules and pentyl groups are shown in VDW representation, white balls - hydrogen atoms, red balls - oxygen atoms, light blue balls - carbon atoms.

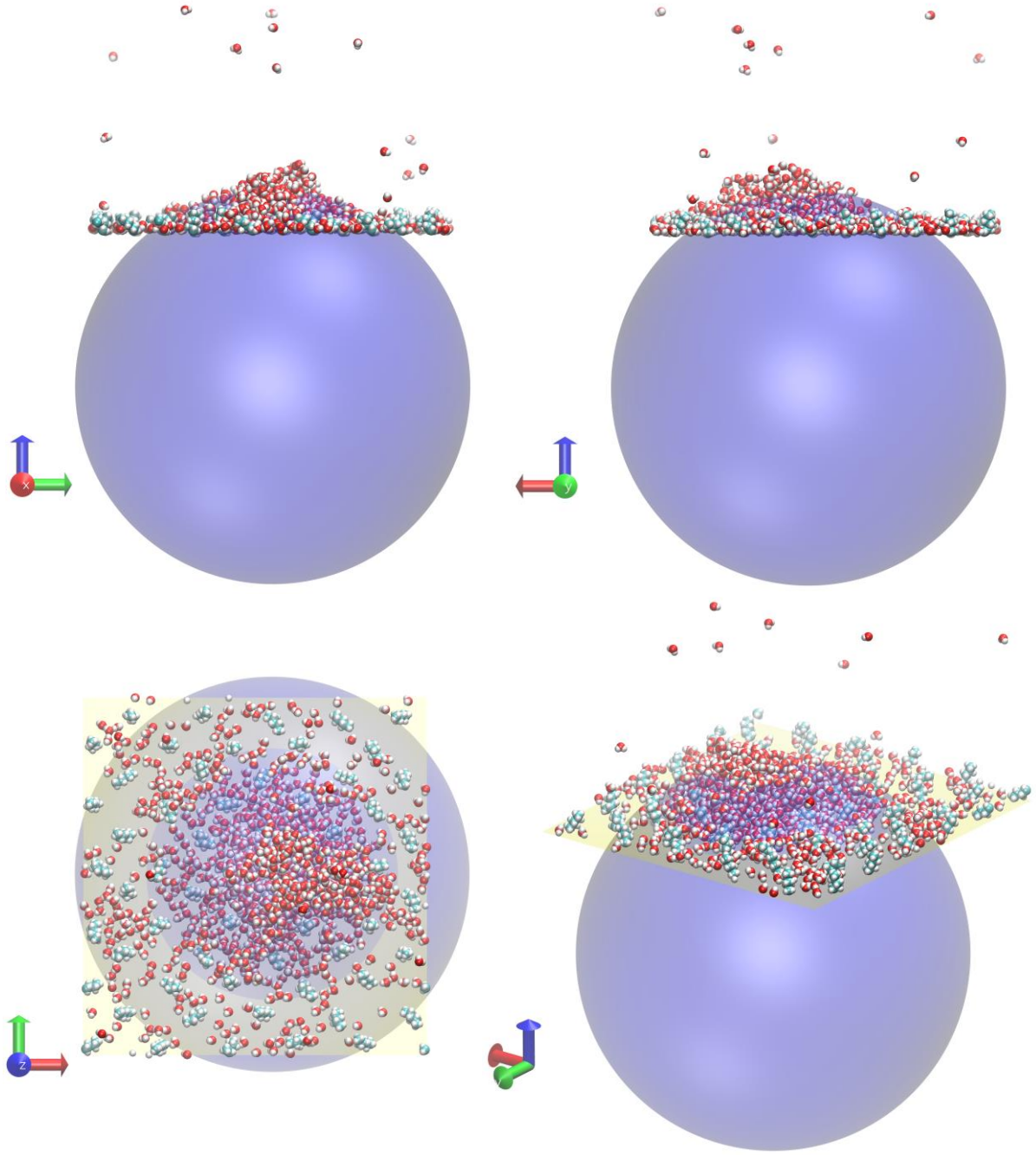

Figure S14. Simulation snapshot of the quartz surface with pentyl concentration 0.579 groups per square nm (surface 2). View along x axis: top left; view along y axis: top right; view along z axis: bottom left; isometric view: bottom right. The sphere fitted to the iso-density chart is illustrated in light purple color. The surface is illustrated with square in light yellow color. Water molecules and pentyl groups are shown in VDW representation, white balls - hydrogen atoms, red balls - oxygen atoms, light blue balls - carbon atoms.

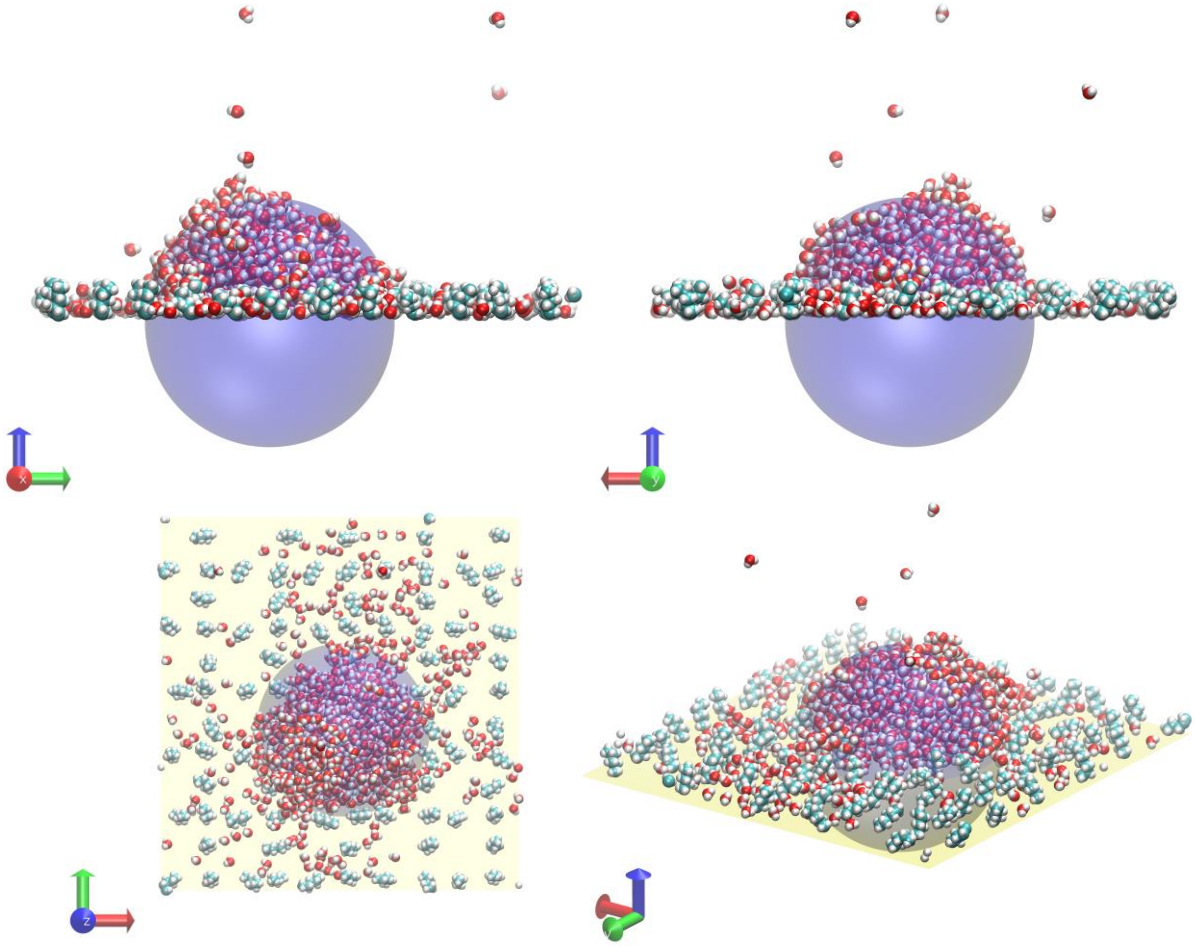

Figure S15. Simulation snapshot of the quartz surface with pentyl concentration 0.868 groups per square nm (surface 3). View along x axis: top left; view along y axis: top right; view along z axis: bottom left; isometric view: bottom right. The sphere fitted to the iso-density chart is illustrated in light purple color. The surface is illustrated with square in light yellow color. Water molecules and pentyl groups are shown in VDW representation, white balls - hydrogen atoms, red balls - oxygen atoms, light blue balls - carbon atoms.

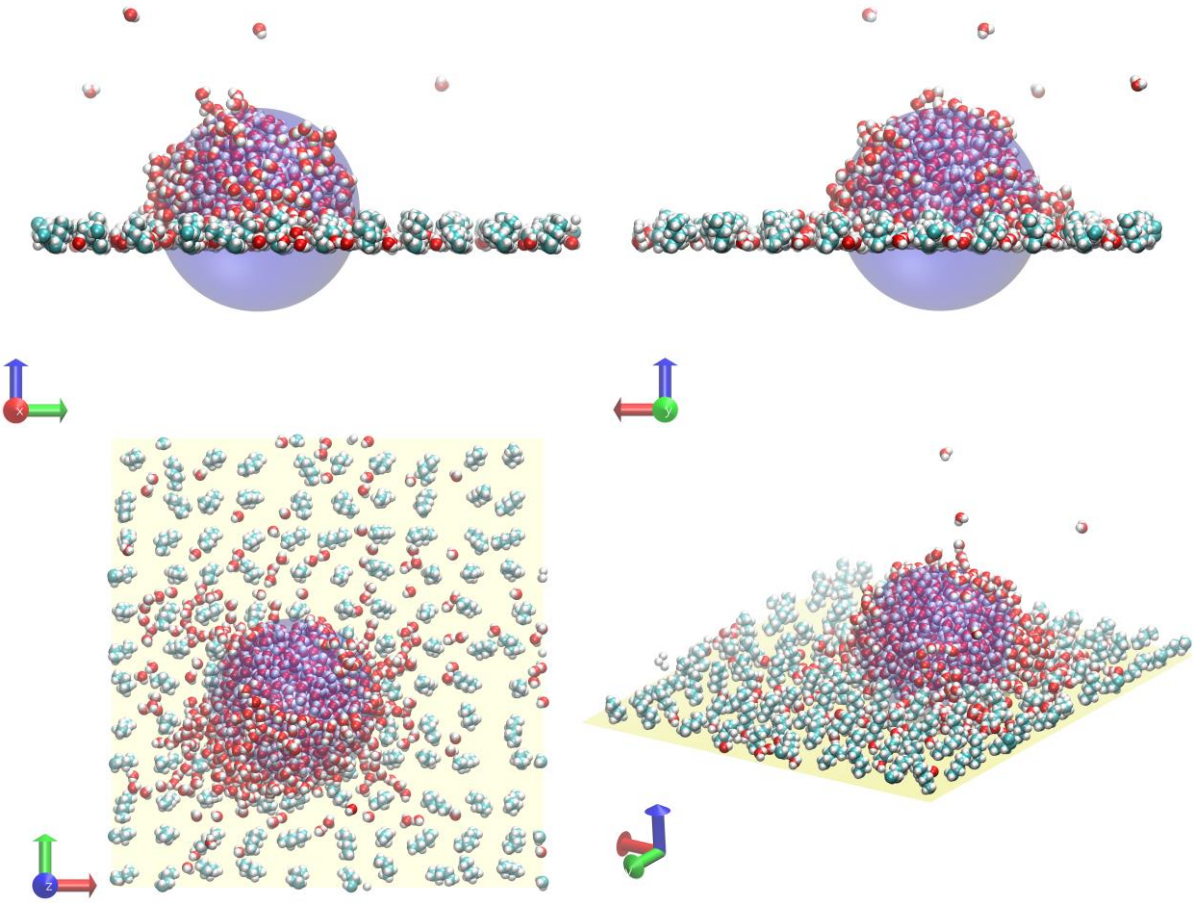

Figure S16. Simulation snapshot of the quartz surface with pentyl concentration 1.157 groups per square nm (surface 4). View along x axis: top left; view along y axis: top right; view along z axis: bottom left; isometric view: bottom right. The sphere fitted to the iso-density chart is illustrated in light purple color. The surface is illustrated with square in light yellow color. Water molecules and pentyl groups are shown in VDW representation, white balls - hydrogen atoms, red balls - oxygen atoms, light blue balls - carbon atoms.

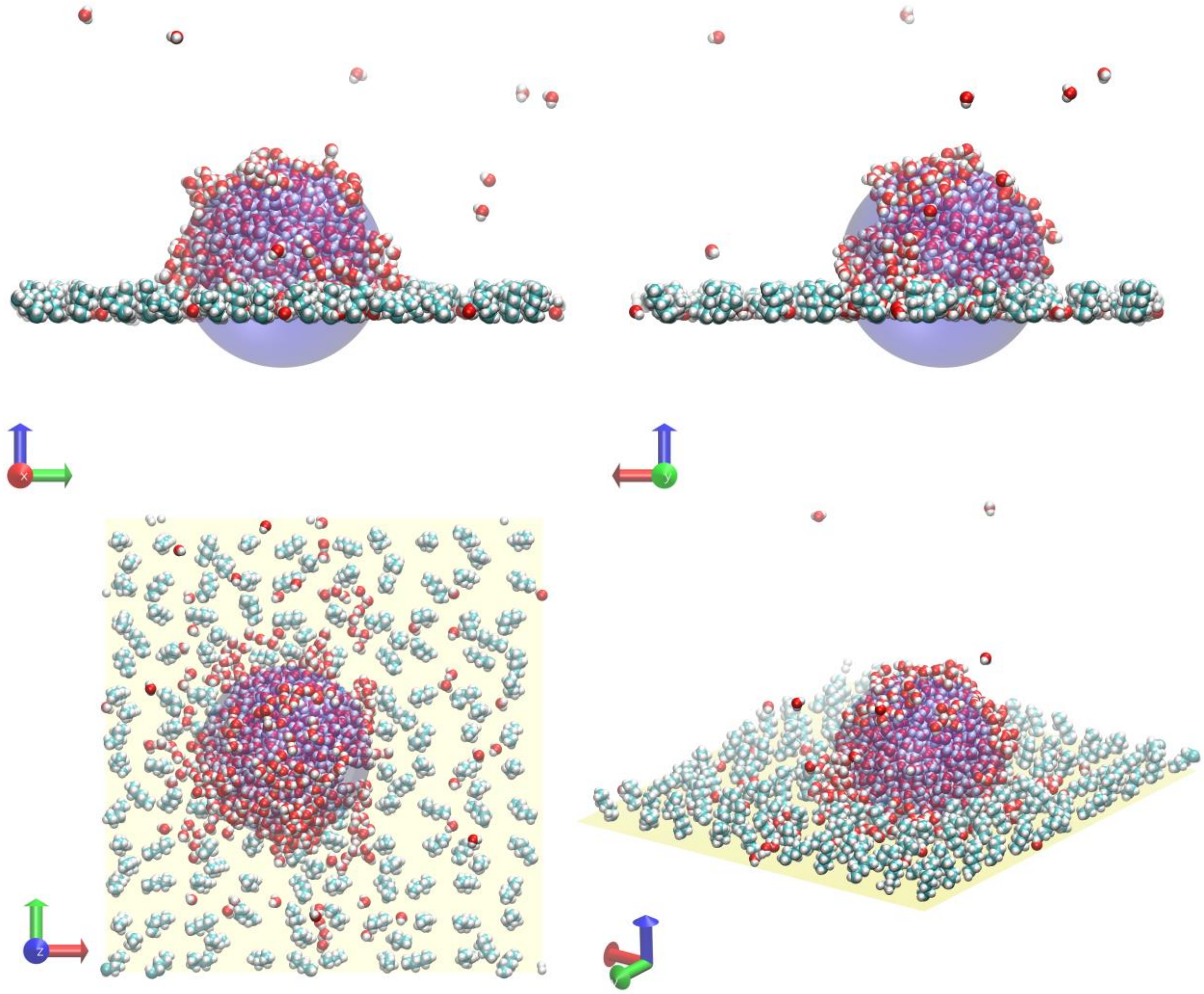

Figure S17. Simulation snapshot of the quartz surface with pentyl concentration 1.447 groups per square nm (surface 5). View along x axis: top left; view along y axis: top right; view along z axis: bottom left; isometric view: bottom right. The sphere fitted to the iso-density chart is illustrated in light purple color. The surface is illustrated with square in light yellow color. Water molecules and pentyl groups are shown in VDW representation, white balls - hydrogen atoms, red balls - oxygen atoms, light blue balls - carbon atoms.

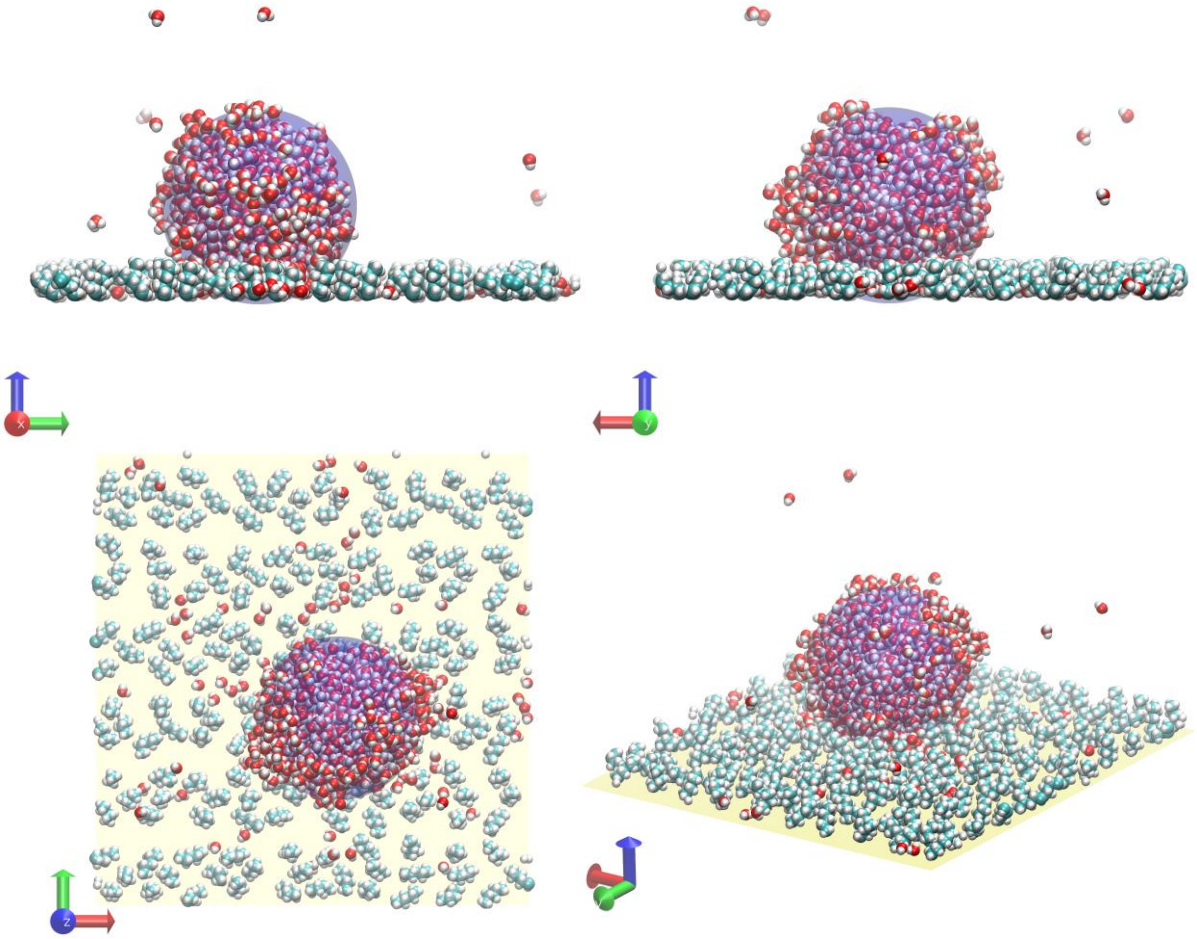

Figure S18. Simulation snapshot of the quartz surface with pentyl concentration 1.736 groups per square nm (surface 6). View along x axis: top left; view along y axis: top right; view along z axis: bottom left; isometric view: bottom right. The sphere fitted to the iso-density chart is illustrated in light purple color. The surface is illustrated with square in light yellow color. Water molecules and pentyl groups are shown in VDW representation, white balls - hydrogen atoms, red balls - oxygen atoms, light blue balls - carbon atoms.

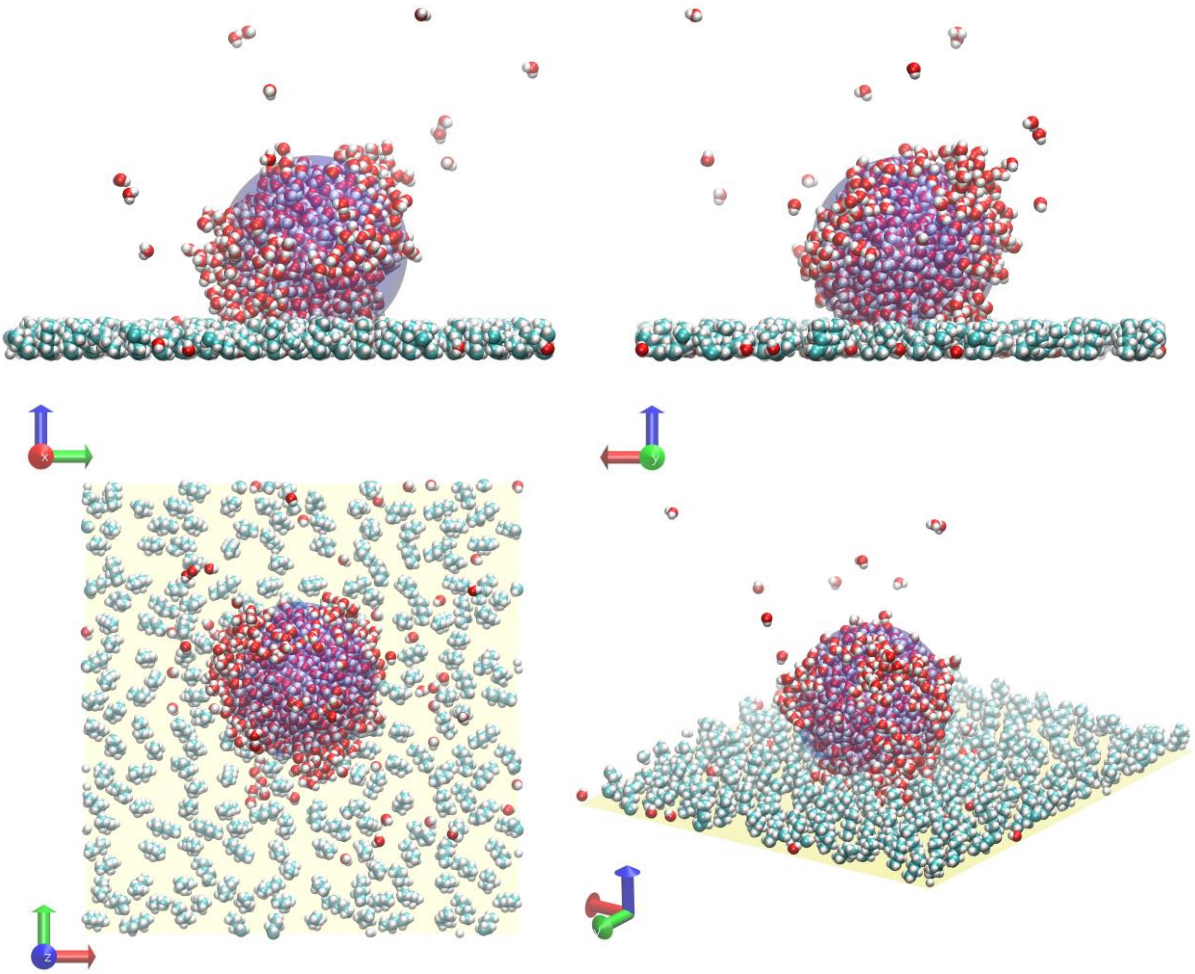

Figure S19. Simulation snapshot of the quartz surface with pentyl concentration 2.025 groups per square nm (surface 7). View along x axis: top left; view along y axis: top right; view along z axis: bottom left; isometric view: bottom right. The sphere fitted to the iso-density chart is illustrated in light purple color. The surface is illustrated with square in light yellow color. Water molecules and pentyl groups are shown in VDW representation, white balls - hydrogen atoms, red balls - oxygen atoms, light blue balls - carbon atoms.

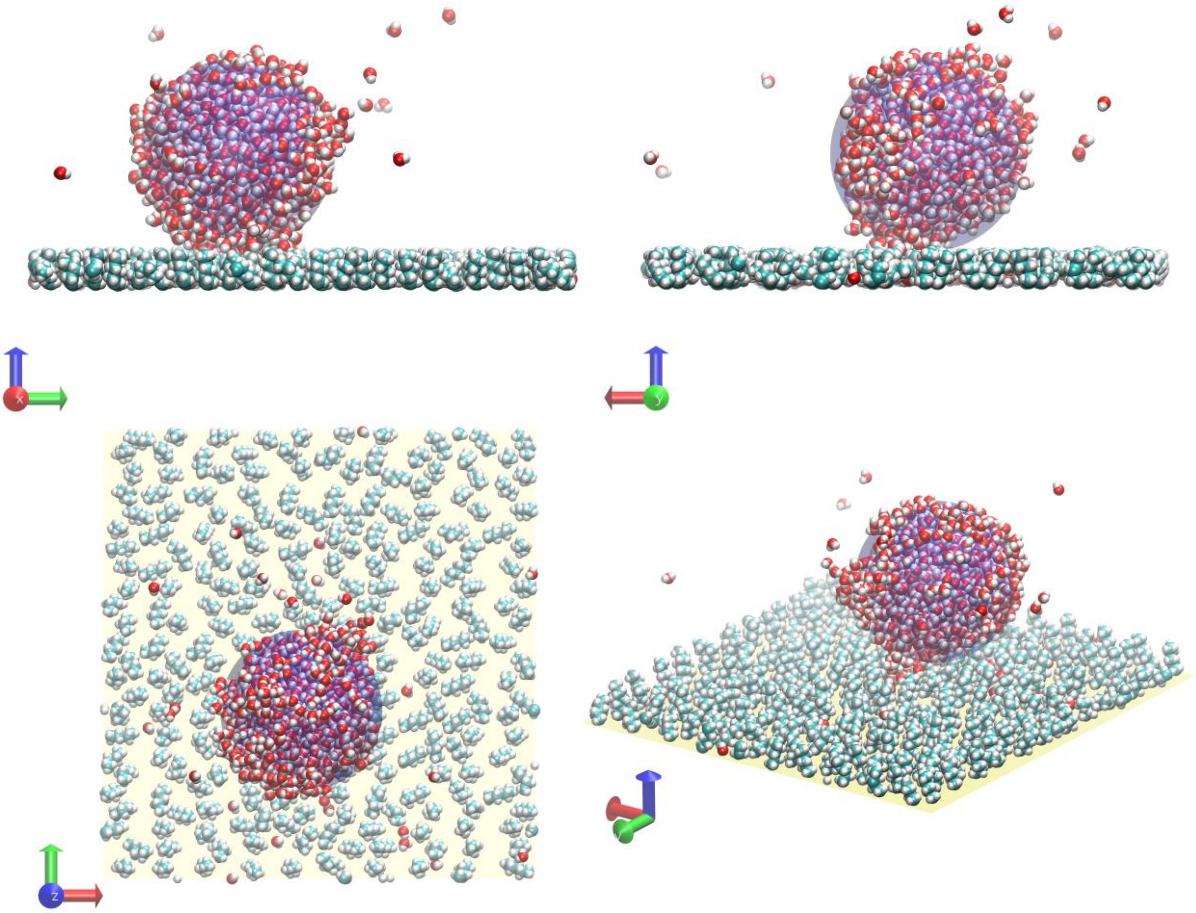

Figure S20. Simulation snapshot of the quartz surface with pentyl concentration 2.314 groups per square nm (surface 8). View along x axis: top left; view along y axis: top right; view along z axis: bottom left; isometric view: bottom right. The sphere fitted to the iso-density chart is illustrated in light purple color. The surface is illustrated with square in light yellow color. Water molecules and pentyl groups are shown in VDW representation, white balls - hydrogen atoms, red balls - oxygen atoms, light blue balls - carbon atoms.

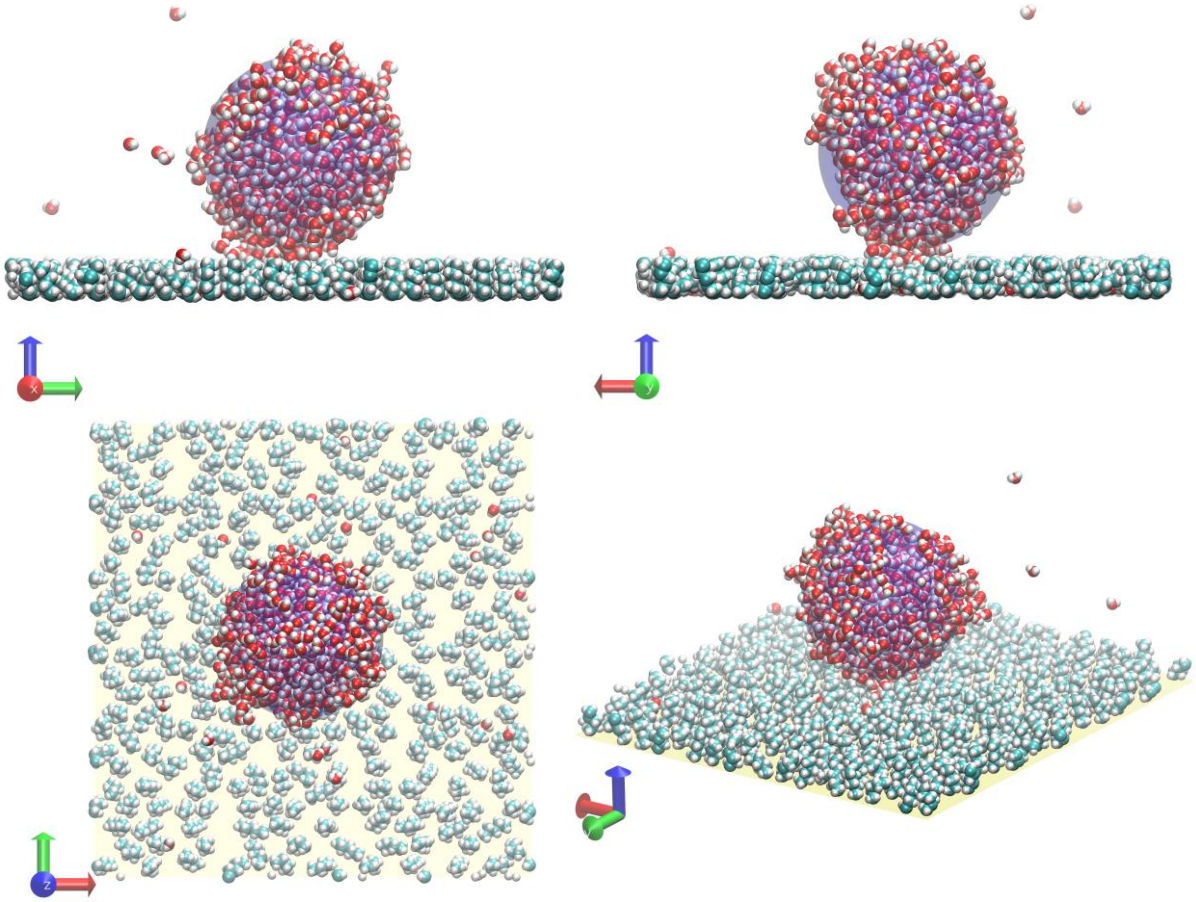

Figure S21. Simulation snapshot of the quartz surface with pentyl concentration 2.604 groups per square nm (surface 9). View along x axis: top left; view along y axis: top right; view along z axis: bottom left; isometric view: bottom right. The sphere fitted to the iso-density chart is illustrated in light purple color. The surface is illustrated with square in light yellow color. Water molecules and pentyl groups are shown in VDW representation, white balls - hydrogen atoms, red balls - oxygen atoms, light blue balls - carbon atoms.

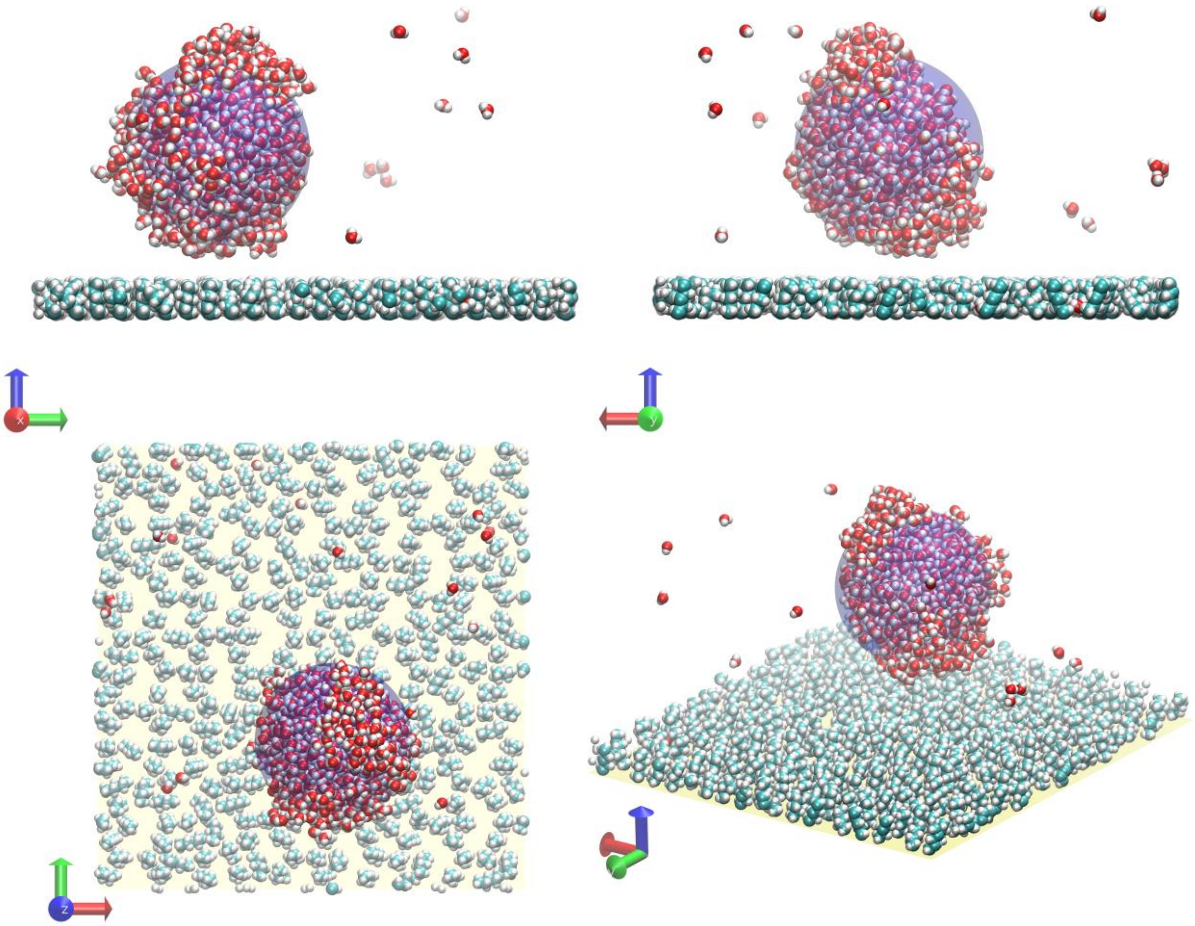

Figure S22. Simulation snapshot of the quartz surface with pentyl concentration 2.893 groups per square nm (surface 10). View along x axis: top left; view along y axis: top right; view along z axis: bottom left; isometric view: bottom right. The sphere fitted to the iso-density chart is illustrated in light purple color. The surface is illustrated with square in light yellow color. Water molecules and pentyl groups are shown in VDW representation, white balls - hydrogen atoms, red balls - oxygen atoms, light blue balls - carbon atoms.

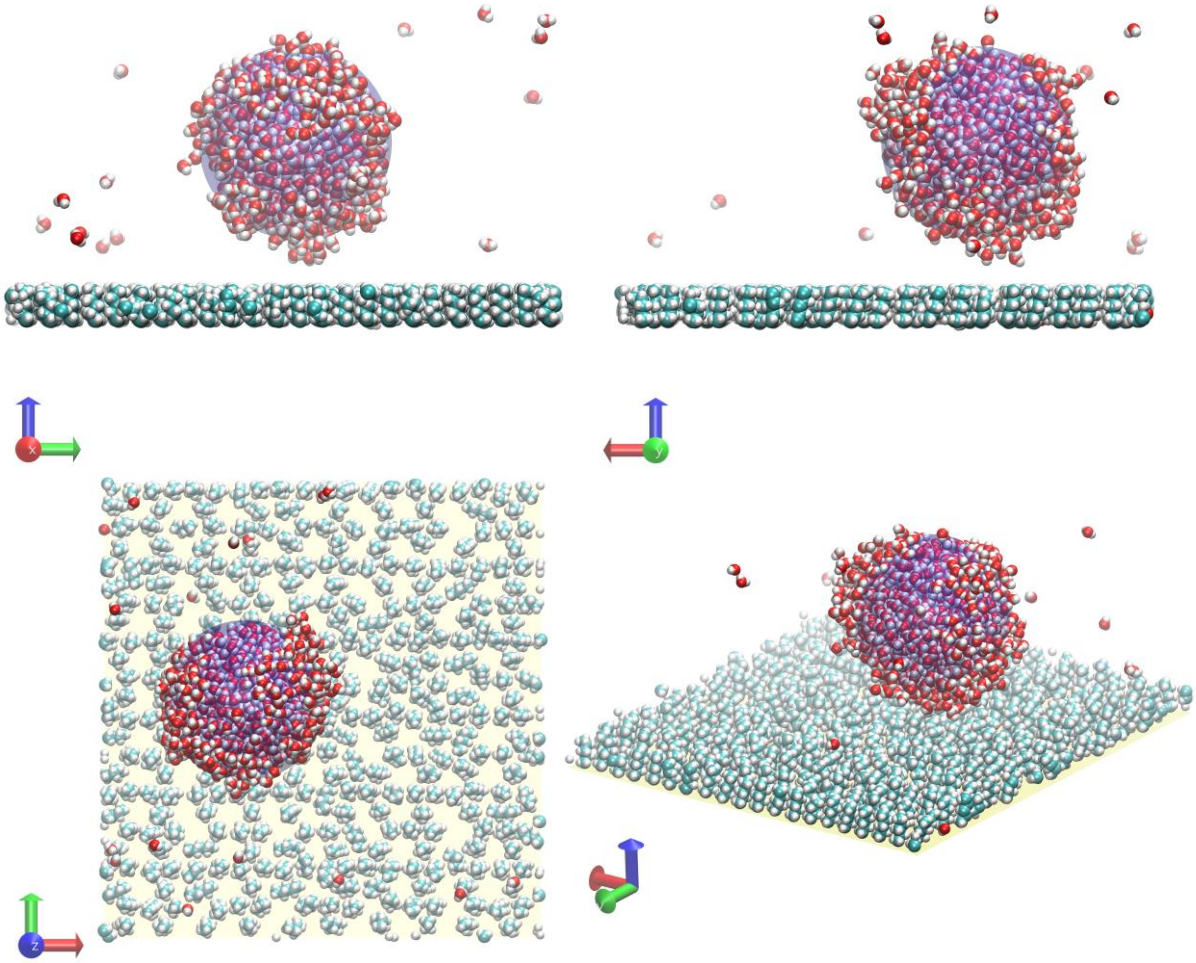

Figure S23. Simulation snapshot of the quartz surface with pentyl concentration 3.182 groups per square nm (surface 11). View along x axis: top left; view along y axis: top right; view along z axis: bottom left; isometric view: bottom right. The sphere fitted to the iso-density chart is illustrated in light purple color. The surface is illustrated with square in light yellow color. Water molecules and pentyl groups are shown in VDW representation, white balls - hydrogen atoms, red balls - oxygen atoms, light blue balls - carbon atoms.

Simulation Snapshots with Removed Pentyl Groups for Surfaces 1 Through 11

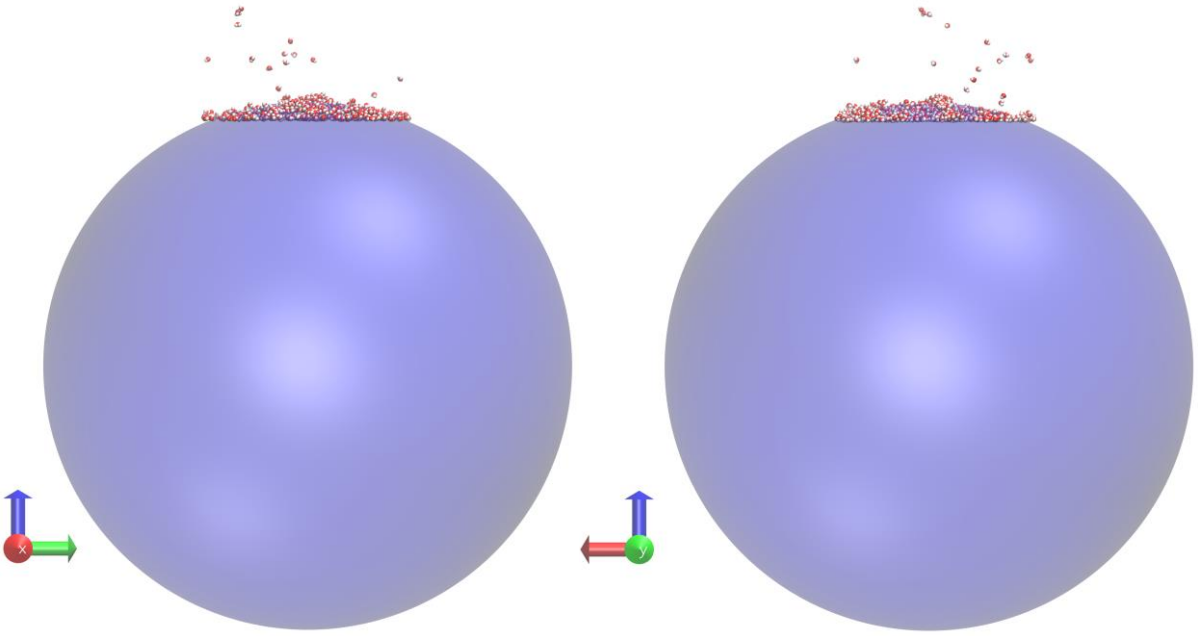

Figure S24. Side views of a water droplet on the quartz surface with removed pentyl groups for pentyl concentration 0.289 groups per square nm (surface 1). View along x axis: left; view along y axis: right. The sphere fitted to the iso-density chart is illustrated in light purple color. The surface position is indicated by the lowest laying water molecules. Water molecules are shown in VDW representation, white balls - hydrogen atoms, red balls - oxygen atoms.

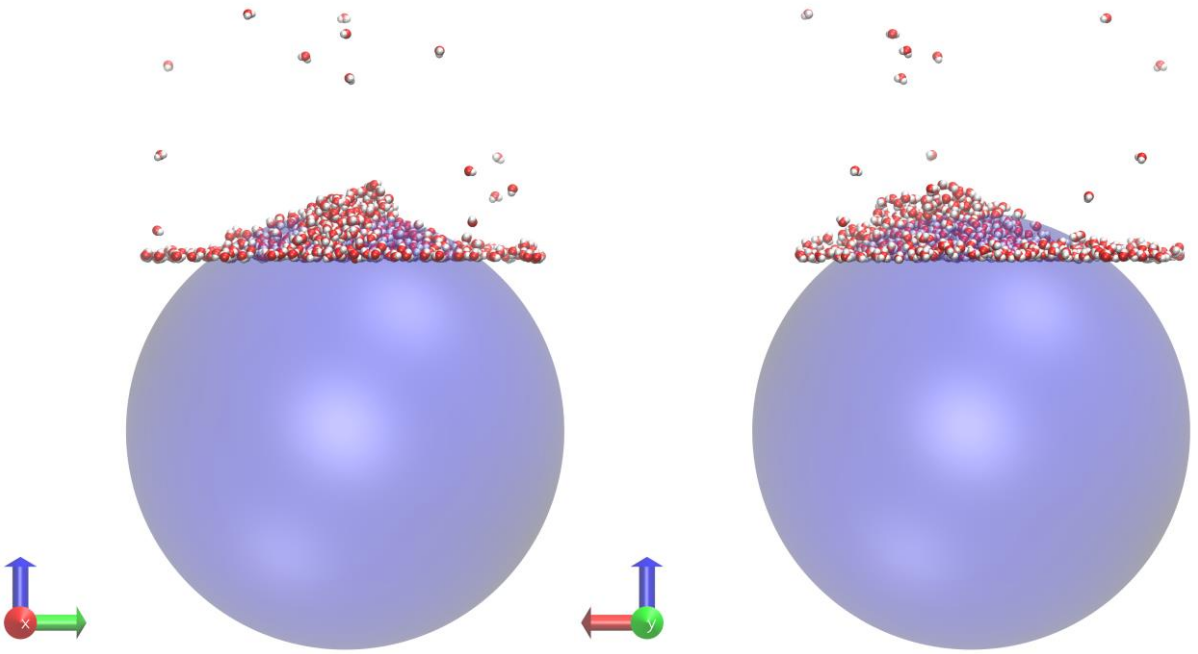

Figure S25. Side views of a water droplet on the quartz surface with removed pentyl groups for pentyl concentration 0.579 groups per square nm (surface 2). View along x axis: left; view along y axis: right. The sphere fitted to the iso-density chart is illustrated in light purple color. The surface position is indicated by the lowest laying water molecules. Water molecules are shown in VDW representation, white balls - hydrogen atoms, red balls - oxygen atoms.

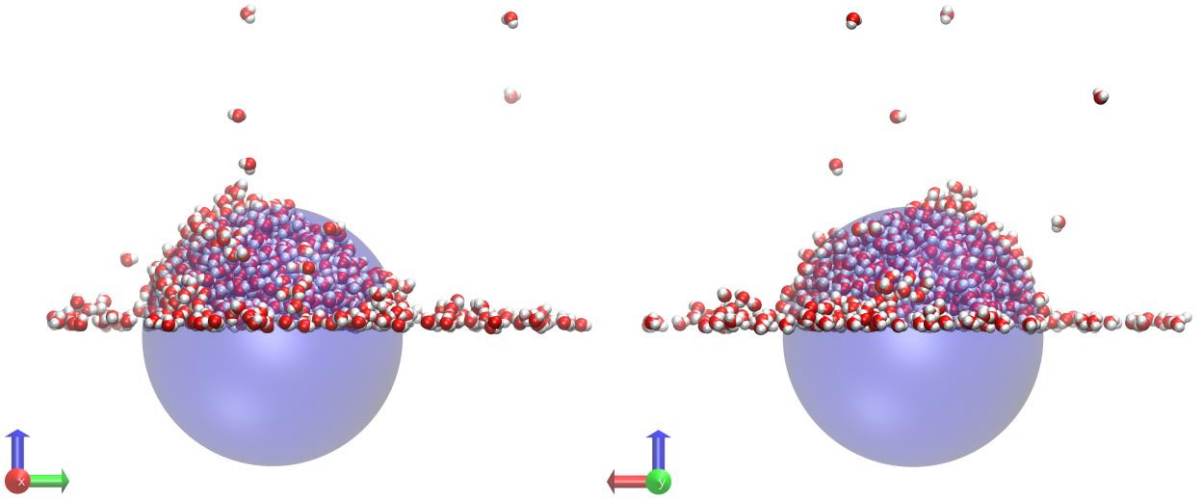

Figure S26. Side views of a water droplet on the quartz surface with removed pentyl groups for pentyl concentration 0.868 groups per square nm (surface 3). View along x axis: left; view along y axis: right. The sphere fitted to the iso-density chart is illustrated in light purple color. The surface position is indicated by the lowest laying water molecules. Water molecules are shown in VDW representation, white balls - hydrogen atoms, red balls - oxygen atoms.

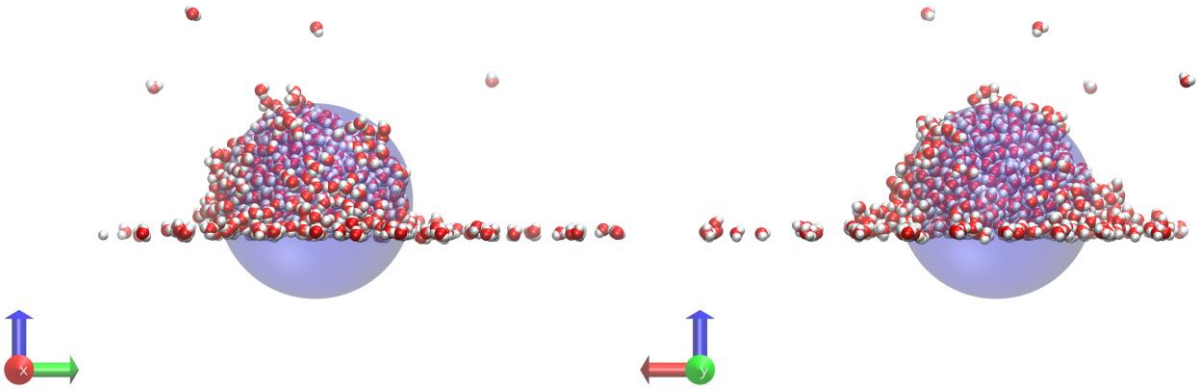

Figure S27. Side views of a water droplet on the quartz surface with removed pentyl groups for pentyl concentration 1.157 groups per square nm (surface 4). View along x axis: left; view along y axis: right. The sphere fitted to the iso-density chart is illustrated in light purple color. The surface position is indicated by the lowest laying water molecules. Water molecules are shown in VDW representation, white balls - hydrogen atoms, red balls - oxygen atoms.

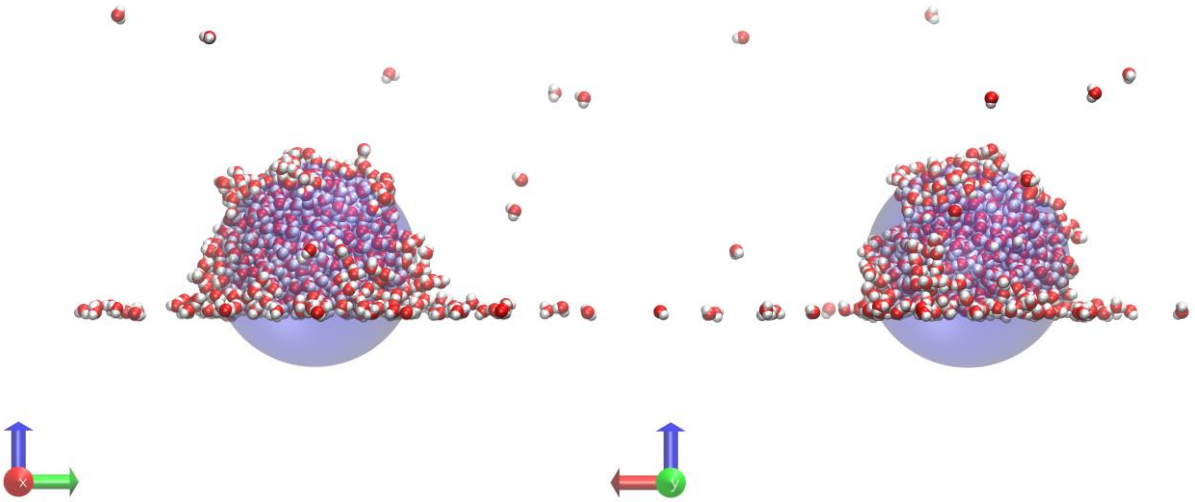

Figure S28. Side views of a water droplet on the quartz surface with removed pentyl groups for pentyl concentration 1.447 groups per square nm (surface 5). View along x axis: left; view along y axis: right. The sphere fitted to the iso-density chart is illustrated in light purple color. The surface position is indicated by the lowest laying water molecules. Water molecules are shown in VDW representation, white balls - hydrogen atoms, red balls - oxygen atoms.

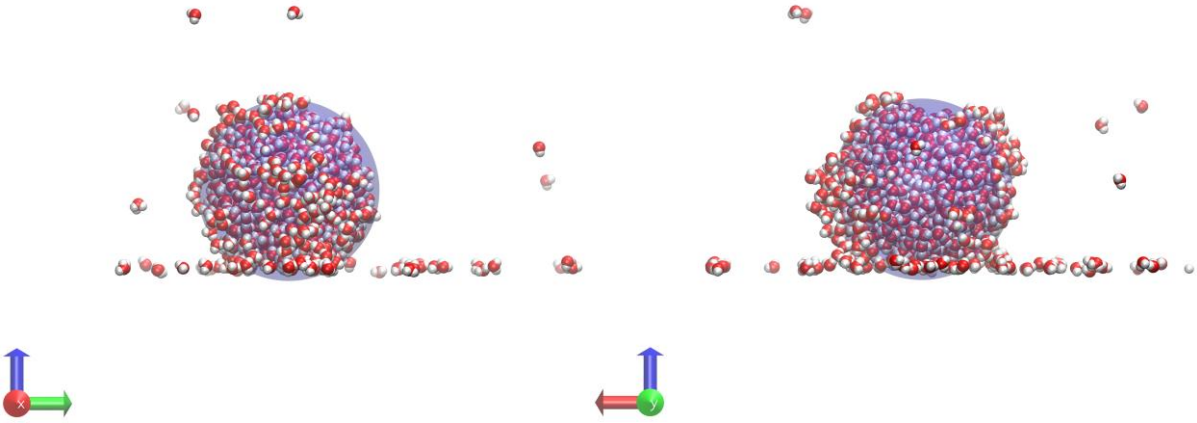

Figure S29. Side views of a water droplet on the quartz surface with removed pentyl groups for pentyl concentration 1.736 groups per square nm (surface 6). View along x axis: left; view along y axis: right. The sphere fitted to the iso-density chart is illustrated in light purple color. The surface position is indicated by the lowest laying water molecules. Water molecules are shown in VDW representation, white balls - hydrogen atoms, red balls - oxygen atoms.

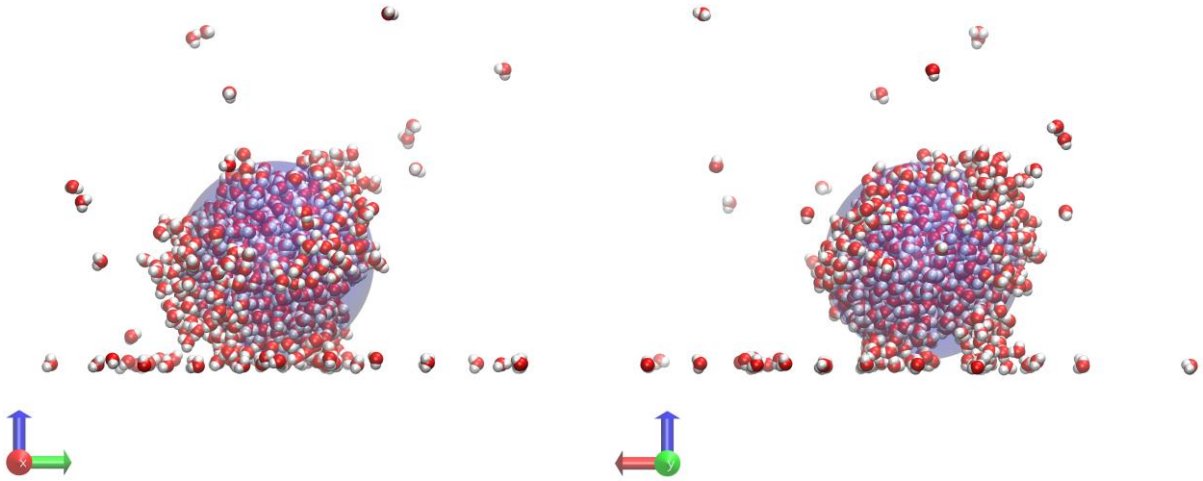

Figure S30. Side views of a water droplet on the quartz surface with removed pentyl groups for pentyl concentration 2.025 groups per square nm (surface 7). View along x axis: left; view along y axis: right. The sphere fitted to the iso-density chart is illustrated in light purple color. The surface position is indicated by the lowest laying water molecules. Water molecules are shown in VDW representation, white balls - hydrogen atoms, red balls - oxygen atoms.

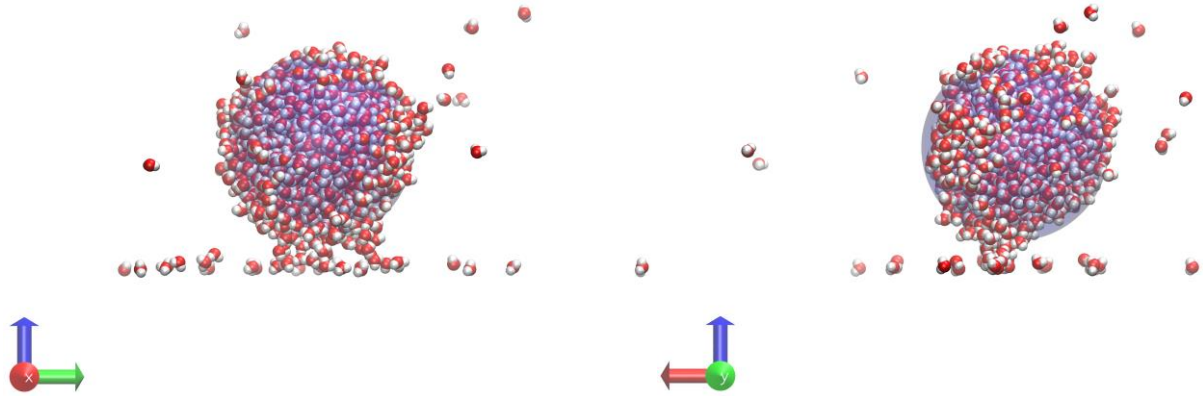

Figure S31. Side views of a water droplet on the quartz surface with removed pentyl groups for pentyl concentration 2.314 groups per square nm (surface 8). View along x axis: left; view along y axis: right. The sphere fitted to the iso-density chart is illustrated in light purple color. The surface position is indicated by the lowest laying water molecules. Water molecules are shown in VDW representation, white balls - hydrogen atoms, red balls - oxygen atoms.

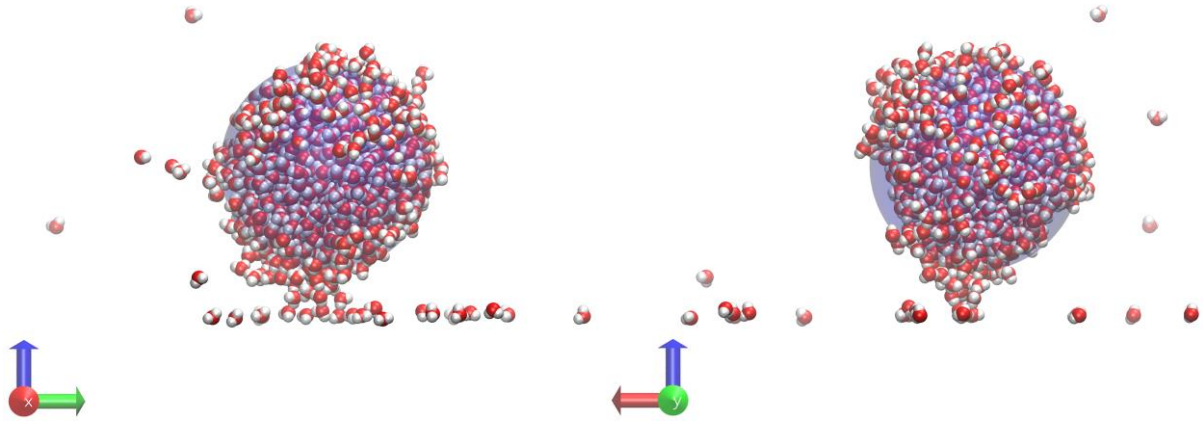

Figure S32. Side views of a water droplet on the quartz surface with removed pentyl groups for pentyl concentration 2.604 groups per square nm (surface 9). View along x axis: left; view along y axis: right. The

sphere fitted to the iso-density chart is illustrated in light purple color. The surface position is indicated by the lowest laying water molecules. Water molecules are shown in VDW representation, white balls - hydrogen atoms, red balls - oxygen atoms.

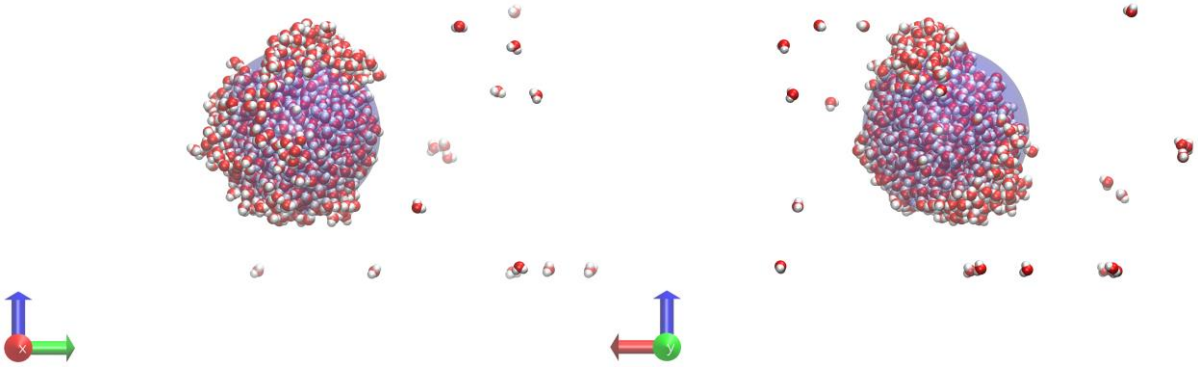

Figure S33. Side views of a water droplet on the quartz surface with removed pentyl groups for pentyl concentration 2.893 groups per square nm (surface 10). View along x axis: left; view along y axis: right. The sphere fitted to the iso-density chart is illustrated in light purple color. The surface position is indicated by the lowest laying water molecules. Water molecules are shown in VDW representation, white balls - hydrogen atoms, red balls - oxygen atoms.

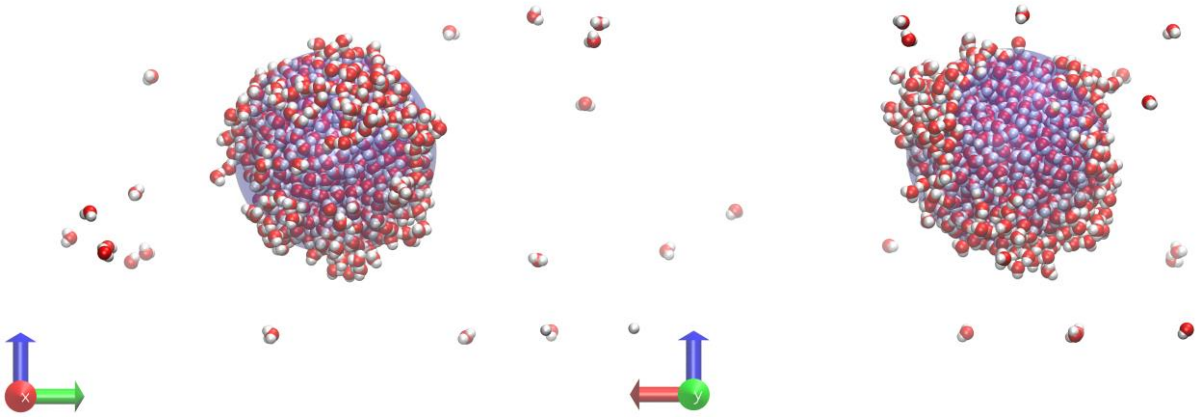

Figure S34. Side views of a water droplet on the quartz surface with removed pentyl groups for pentyl concentration 3.182 groups per square nm (surface 11). View along x axis: left; view along y axis: right. The sphere fitted to the iso-density chart is illustrated in light purple color. The surface position is indicated by the lowest laying water molecules. Water molecules are shown in VDW representation, white balls - hydrogen atoms, red balls - oxygen atoms.